

8-20-2024

## LaCoO<sub>3</sub> is a promising catalyst for dry reforming of benzene used as a surrogate of biomass tar

BAŞAR ÇAĞLAR

DENİZ ÜNER

Follow this and additional works at: <https://journals.tubitak.gov.tr/chem>

 Part of the [Chemistry Commons](#)

### Recommended Citation

ÇAĞLAR, BAŞAR and ÜNER, DENİZ (2024) "LaCoO<sub>3</sub> is a promising catalyst for dry reforming of benzene used as a surrogate of biomass tar," *Turkish Journal of Chemistry*. Vol. 48: No. 4, Article 10.

<https://doi.org/10.55730/1300-0527.3685>

Available at: <https://journals.tubitak.gov.tr/chem/vol48/iss4/10>



This work is licensed under a [Creative Commons Attribution 4.0 International License](#).

This Research Article is brought to you for free and open access by TÜBİTAK Academic Journals. It has been accepted for inclusion in Turkish Journal of Chemistry by an authorized editor of TÜBİTAK Academic Journals. For more information, please contact [pinar.dundar@tubitak.gov.tr](mailto:pinar.dundar@tubitak.gov.tr).

## LaCoO<sub>3</sub> is a promising catalyst for the dry reforming of benzene used as a surrogate of biomass tar

Başar ÇAĞLAR<sup>1,\*</sup> , Deniz ÜNER<sup>1,2</sup> 

<sup>1</sup>Department of Energy Systems Engineering, Faculty of Engineering, İzmir Institute of Technology, İzmir, Türkiye

<sup>2</sup>Department of Chemical Engineering, Faculty of Engineering, Middle East Technical University, Ankara, Türkiye

Received: 11.03.2024 • Accepted/Published Online: 15.06.2024 • Final Version: 20.08.2024

**Abstract:** Tar build-up is one of the bottlenecks of biomass gasification processes. Dry reforming of tar is an alternative solution if the oxygen chemical potential on the catalyst surface is at a sufficient level. For this purpose, an oxygen-donor perovskite, LaCoO<sub>3</sub>, was used as a catalyst for the dry reforming of tar. To circumvent the complexity of the tar and its constituents, the benzene molecule was chosen as a model compound. Dry reforming of benzene vapor on the LaCoO<sub>3</sub> catalyst was investigated at temperatures of 600, 700, and 800 °C; at CO<sub>2</sub>/C<sub>6</sub>H<sub>6</sub> ratios of 3, 6, and 12; and at space velocities of 14,000 and 28,000 h<sup>-1</sup>. The conventional Ni(15 wt.%)/Al<sub>2</sub>O<sub>3</sub> catalyst was also used as a reference material to determine the relative activity of the LaCoO<sub>3</sub> catalyst. Different characterization techniques such as X-ray diffraction, N<sub>2</sub> adsorption-desorption, temperature-programmed reduction, and oxidation were used to determine the physicochemical characteristics of the catalysts. The findings demonstrated that the LaCoO<sub>3</sub> catalyst has higher CO<sub>2</sub> conversion, higher H<sub>2</sub> and CO yields, and better stability than the Ni(15 wt.%)/γ-Al<sub>2</sub>O<sub>3</sub> catalyst. The improvement in activity was attributed to the strong capacity of LaCoO<sub>3</sub> for oxygen exchange. The transfer of lattice oxygen from the surface of the LaCoO<sub>3</sub> catalyst facilitates the oxidation of carbon and other surface species and leads to higher conversion and yields.

**Key words:** Biomass gasification, tar removal, H<sub>2</sub> production, dry reforming, benzene, LaCoO<sub>3</sub> catalyst

### 1. Introduction

Biomass is the only renewable source of useful carbon, which can be used directly to replace fossil fuels for fuel and chemical production [1–4]. Among biomass resources, lignocellulosic biomass is the most attractive type of feedstock for producing biofuels and chemicals [5] due to its abundance, low-cost, and nonedible character. For the valorization of lignocellulosic biomass, the conversion of lignin has remained a challenge due to its inactive chemical nature. The lignin content of lignocellulosic biomass varies between 10 and 35 wt.%, which corresponds to up to 40% energy content of the biomass [6]. Therefore, the effective utilization of lignin has great significance for the economic performance of lignocellulosic biomass conversion. Gasification is one of the techniques enabling lignin to be processed along with the other components of lignocellulosic feedstock to produce fuels and chemicals. In gasification, lignocellulosic biomass is converted into a gas mixture at relatively high temperatures (600–1100 °C) in an oxygen-deficient environment. The main drawback of gasification is the undesired tar formation during the process. Tar consists of a mixture of organic compounds [7], including primarily alkylated aromatics, phenolic compounds, and polycyclic aromatic hydrocarbons (PAHs) [8,9]. Tar causes severe problems in downstream applications of biomass gasification processes as it blocks fuel lines and injectors in internal combustion engines, plugs compressors and transfer lines in combined-cycle plants, and poisons fuel cell catalysts (e.g., Pt/C) and Fischer–Tropsch catalysts (e.g., Fe-Co/Al<sub>2</sub>O<sub>3</sub>). In addition to these problems, tar formation leads to decreased efficiency of biomass gasification processes due to incomplete carbon conversion [10]. For the successful development of efficient gasification technology, tar removal or conversion is required.

Catalytic steam and dry reforming are attractive methods used for tar removal since they retain the chemical energies of tar compounds in the product gas, consisting mainly of H<sub>2</sub> and CO, and provide an opportunity to adjust the composition of the product gas [7]. Although catalytic steam reforming of tar has been addressed more in the literature compared to catalytic dry reforming, the latter has been receiving increased attention recently since it allows

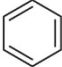
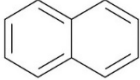
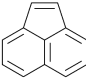
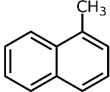
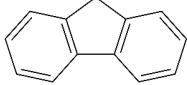
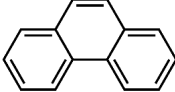
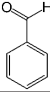
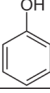
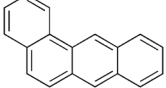
\* Correspondence: basarcaglar@iyte.edu.tr

the use of CO<sub>2</sub> as a feedstock. This is important because CO<sub>2</sub> concentrations in the gasifier outlet (15–20 vol.%) are significantly higher than H<sub>2</sub>O concentrations [11]. Therefore, a dry reforming process also allows both tar removal and CO<sub>2</sub> valorization.

Tar has a complex chemical nature due to a wide range of chemical compounds (e.g., benzene, naphthalene, acenaphthylene, methylnaphthalene, fluorene, phenanthrene, benzaldehyde, phenols, naphthofurans, benzanthracene, and pyrene). To bypass the complexity of tar and gain further insight into tar decomposition chemistry, various model tar compounds have been extensively studied. Among these studied model tar compounds, toluene, xylene, and styrene were used to represent alkylated aromatics, phenol and cresol were used for phenolic compounds, and benzene and naphthalene were used for aromatic hydrocarbons [12,13]. Among model compounds, benzene has received more attention since it constitutes the largest proportion of tar compositions, specifically for fixed-bed downdraft and fluidized bed gasifiers, while most other compounds are benzene derivatives [14–16]. The benzene ring is a common feature seen in the molecular structure of tar compounds due to its high thermal stability (Table 1) [15,17–19]. Benzene shows higher thermal stability (T<sub>dec</sub> > 1400 °C) than naphthalene (T<sub>dec</sub> > 1300 °C) and its other high-molecular-weight derivatives [20]. The composition of benzene and its high thermal stability suggest that benzene decomposition plays a crucial role for the complete conversion of biomass tar. In addition, benzene is a suitable model compound for controllable continuous reactant feeding to a reactor due to its low melting point (i.e., liquid state at room temperature) (Table 1), which is important in regulating reactant flow rate and residence time. For these reasons, benzene was selected as a model tar compound in this study to mimic tar chemistry.

CO<sub>2</sub> reforming of tar offers the benefit of simultaneous valorization of both compounds. However, the most important problem is catalyst deactivation due to severe carbon build-up. Ni-based catalysts were generally preferred due to the high reforming activity of nickel. Zheng et al. [21] investigated the catalytic dry reforming of toluene on Ni-containing catalysts on different supports such as MgO,  $\gamma$ -Al<sub>2</sub>O<sub>3</sub>,  $\alpha$ -Al<sub>2</sub>O<sub>3</sub>, SiO<sub>2</sub>, and ZrO<sub>2</sub> at 600 °C at a CO<sub>2</sub>/toluene ratio of 16. They found that the Ni/MgO catalyst exhibited the highest performance with 90% toluene conversion and high stability (5.5%

**Table 1.** Typical tar compounds observed at gasification outlet.

Chemical compound	Chemical structure	Boiling point (°C)	Melting point (°C)
Benzene		80.1	5.53
Naphthalene		218.0	78.2
Acenaphthylene		280.0	91.8
Methylnaphthalene		240.0	-22.0
Fluorene		295.0	116.0
Phenanthrene		332.0	101
Benzaldehyde		178.1	-57.0
Phenol		181.7	40.5
Benzanthracene		438.0	158

activity loss in 400 min). This was attributed to the strong interactions between Ni and MgO due to the Ni-Mg-O solid solution and the high dispersion of Ni (low particle size of Ni) on the MgO support. Laosiripojana et al. [22] also tested a Ni-based catalyst on different support materials (e.g., MgO-Al<sub>2</sub>O<sub>3</sub>, La<sub>0.8</sub>Ca<sub>0.2</sub>CrO<sub>3</sub>, and La<sub>0.8</sub>Ca<sub>0.2</sub>CrO<sub>3</sub>/MgO-Al<sub>2</sub>O<sub>3</sub>). They used naphthalene as a model compound and analyzed the performance of Ni-Fe bimetallic catalysts. They investigated the effect of catalyst type and CO<sub>2</sub>/naphthalene ratio on the H<sub>2</sub> yield, determining that H<sub>2</sub> yield increased with CO<sub>2</sub>/naphthalene ratios between 0.5 and 2 and remained constant above a CO<sub>2</sub>/naphthalene ratio of 2. The highest H<sub>2</sub> yield was observed as 80% on the Ni-Fe-containing La<sub>0.8</sub>Ca<sub>0.2</sub>CrO<sub>3</sub>/MgO-Al<sub>2</sub>O<sub>3</sub> catalyst at 700 °C. The dry reforming activities of Ni- and Fe-containing catalysts were also tested by Nam et al. [23]. They investigated the benzene dry reforming activity of SiC-supported Ni and NiFe catalysts in a chemical looping system. They observed that the NiFe/SiC catalyst achieved higher benzene conversion (>90% above 730 °C) and higher H<sub>2</sub> yield (7.2% at 840 °C), which was linked to higher benzene activation on the Ni surface. In contrast, Abou Rached et al. [24] analyzed the effects of cerium and lanthanum on Ni-Al catalysts for the dry reforming of toluene. They performed experiments at a CO<sub>2</sub>/toluene ratio of 7 between 300 and 800 °C and found that Ce and La promotion did not affect toluene conversion (e.g., 100% above 450 °C), but they improved the stability of the catalyst by decreasing the carbon deposition. Both CeO<sub>2</sub> and La<sub>2</sub>O<sub>3</sub> are known for their facile oxygen exchange capacity. For example, La<sub>2</sub>O<sub>3</sub>-based catalysts exhibited superior performance for soot oxidation [25]. On the other hand, CeO<sub>2</sub> was a favorite candidate for chemical looping processes [26,27]. Hence, both compounds are widely used as oxygen flux agents during catalysis.

Nickel-free catalysts were also tested for the dry reforming of tar compounds. In an early study, Simell et al. [28] evaluated the benzene dry reforming performance of dolomites (CaMg(CO<sub>3</sub>)<sub>2</sub>) at different CO<sub>2</sub>/benzene ratios and temperatures of 750–900 °C. They observed that the benzene conversion varied between 6% and 15% and the H<sub>2</sub>/CO ratio was between 0.1 and 0.25. Another material tested for the dry reforming of tar compounds is olivine (Mg<sub>2</sub>SiO<sub>4</sub> and Fe<sub>2</sub>SiO<sub>4</sub>). Devi et al. [29] studied the catalytic dry reforming of naphthalene on an olivine catalyst at 900 °C and a CO<sub>2</sub>/naphthalene ratio of approximately 100. They observed 80% naphthalene conversion but did not provide any information on product yields. The dry reforming of tar compounds was also studied on biochar as a catalyst at 800 °C and a CO<sub>2</sub>/toluene ratio of 7 [30]. At the H<sub>2</sub>/CO ratio of 0.4, >95% toluene conversion was observed. It was also found that toluene conversion decreased by 20% after process time of 120 min due to carbon deposition, which blocked the active sites on the biochar. Similar results were obtained in the steam reforming of toluene on the same catalyst.

Several different catalysts were investigated for the dry reforming of tar model compounds under different conditions. Ni-based catalysts show high performance due to their high C-C and C-H bond-breaking activities, although they are prone to coke accumulation on the surface, which induces activity loss in the long run. Similar problems were also observed for non-Ni catalysts. To solve the coke deposition problem, La was employed in the catalyst formulation [24]. Rh-promoted LaCoO<sub>3</sub> on a  $\gamma$ -Al<sub>2</sub>O<sub>3</sub> support was found to have high activity for the steam reforming of a biomass-pyrolysis gas mixture as well as high resistance to coke deposition [31–34]. In related studies, the individual effects of Rh and LaCoO<sub>3</sub> on activity and stability were not clearly identified. Given that process economy is significantly affected by the noble metal content of catalysts, it would be interesting to learn more about the performance of noble metal-free LaCoO<sub>3</sub> for reforming reactions. In addition, LaCoO<sub>3</sub> showed high activity towards CO<sub>2</sub> activation for propane dry reforming [35], reverse water-gas shift reaction [36], and CO<sub>2</sub> reduction to CO [37] due to its high oxygen exchange capacity. For these reasons, LaCoO<sub>3</sub> was chosen as a catalyst material in the present study and the catalytic dry reforming of benzene was studied on LaCoO<sub>3</sub> perovskites, which has not been addressed in the literature to date.

In this study, the dry reforming of benzene on the LaCoO<sub>3</sub> catalyst was investigated and the activity was compared against a Ni(15 wt.%)/ $\gamma$ -Al<sub>2</sub>O<sub>3</sub> catalyst, which is a typical tar reforming catalyst formulation used in industrial and academic research [7,38–43]. Both catalysts were characterized by X-ray diffraction (XRD), N<sub>2</sub> adsorption, and temperature-programmed reduction (TPR) and oxidation (TPO) techniques. Dry reforming experiments were conducted for both catalysts in a tubular quartz reactor and the effects of temperature, CO<sub>2</sub>/C<sub>6</sub>H<sub>6</sub> ratio, and flow rate were studied. This research will assist in explorations of the potential of LaCoO<sub>3</sub> as a dry reforming catalyst and the development of new catalyst formulations with high activity, selectivity, and stability to replace conventional Ni/ $\gamma$ -Al<sub>2</sub>O<sub>3</sub> catalysts.

## 2. Experimental

### 2.1. Catalyst preparation

LaCoO<sub>3</sub> was prepared by the citrate-based Pechini method due to its advantages over other synthesis methods such as small particle size, high porosity, better control of stoichiometry, homogeneous distribution of ions, relatively low synthesis temperature, and the use of low-cost precursors [44–46]. La<sub>2</sub>O<sub>3</sub> (99.9%), Co(NO<sub>3</sub>)<sub>2</sub>·6H<sub>2</sub>O (99.9%), citric acid (99.5%), and nitric acid (AR, 60%) were used as starting materials. In the first step, 1.33 g of La<sub>2</sub>O<sub>3</sub> was dissolved in 5 mL of nitric acid

solution and converted to lanthanum nitrate. This nitrate solution was mixed with 2.37 g of cobalt nitrate dissolved in 10 mL of pure water for an atomic ratio of La:Co = 1:1 (LCO). Subsequently, 6.83 g of citric acid was added to this mixture and left to evaporate by stirring for 1 h at 50 °C. At the end of this process, a stable lanthanum cobalt-containing citric acid structure was formed. After 1 h, ethylene glycol was added. The solution was heated to 75 °C with continuous stirring to remove water and accelerate the polyesterification reaction between ethylene glycol and citric acid. After the evaporation of nitrogen-containing gases at this temperature, the remaining material was cooled to room temperature. After this process, a purple viscous solid-liquid mixture was formed. This mixture was turned into a dry gel by heating it to 80 °C in an oven. After drying, the resulting powder was first heated to 350 °C with a heating rate of 10 °C/min and kept at that temperature for 3 h, then heated to 650 °C with a heating rate of 10 °C/min and held for 5 h (Supplementary information, Table S and Figure S1, for an explanation of the two-step calcination). At the end of calcination, LaCoO<sub>3</sub> nanoparticles were obtained.

In this study, Ni(15 wt.)/ $\gamma$ -Al<sub>2</sub>O<sub>3</sub> was used as a reference material to determine the relative activity of LaCoO<sub>3</sub>. The nickel composition was specifically selected considering the composition reported in the literature for commercial catalysts used for tar reforming [7,38–43]. Nickel loading on  $\gamma$ -Al<sub>2</sub>O<sub>3</sub> material was done by incipient wetness impregnation method as suggested by industrial and academic research [18,19,38]. In this method, 1.48 g of nickel nitrate (Ni(NO<sub>3</sub>)<sub>2</sub>·6H<sub>2</sub>O; Merck, Darmstadt, Germany) was dissolved in an excess amount of pure water (5 mL) and added to  $\gamma$ -Al<sub>2</sub>O<sub>3</sub> powder (2 g) dropwise under stirring. The resulting mixture was mixed with a magnetic stirrer for 2 h at room temperature. After the mixing process was completed, the material was kept in an oven at 110 °C overnight. Subsequently, the dehydrated materials were left for calcination at 600 °C for 2 h, which allowed the removal of nitrate species (Supplementary information, Figure S2). After calcination, the nitrate-free material was allowed to cool at room temperature and the process was completed.

## 2.2. Catalyst characterization

The crystal structure and size were determined by XRD analysis. XRD spectra were obtained using a Rigaku Ultima Instrument (Rigaku, Tokyo, Japan) with Cu-K $\alpha$  radiation ( $\lambda$  = 0.154 nm) between 20° and 75° with a scanning rate of 0.1°/s. The average crystalline size was calculated from the Debye–Scherrer formula:

$$L = \frac{0.9\lambda_{K\alpha 1}}{B_{2\theta} \cdot \cos\theta_{max}} \quad (1)$$

Here, L is the average crystalline size,  $\lambda_{K\alpha 1}$  is the wavelength of the X-rays (1.540598 Å for Cu-K<sub>α1</sub> radiation),  $B_{2\theta}$  is the full width at half maximum of the peak, and  $\theta_{max}$  is the angle at maximum.

Surface area, pore volume, and average pore size of the catalysts were determined by N<sub>2</sub> adsorption-desorption at 77 K using a Micromeritics TriStar II instrument (Micromeritics, Norcross, GA, USA). Samples were outgassed at 120 °C for 12 h prior to the experiments.

The reduction and oxidation behaviors of the catalysts were investigated by TPR and TPO experiments in a Micromeritics Chemisorb 2720 instrument. The TPR and TPO experiments were conducted between 25 and 900 °C under the flow of H<sub>2</sub> in Ar (10% H<sub>2</sub>) and O<sub>2</sub> in He (2% O<sub>2</sub>) with a heating rate of 5 °C/min. H<sub>2</sub> and O<sub>2</sub> consumptions were monitored by a thermal conductivity detector. The quantification of H<sub>2</sub> consumption was performed using peak areas and the calibration factor determined by the reference Ag<sub>2</sub>O reduction reaction.

## 2.3. Dry reforming tests

Catalytic tests were performed in a fixed-bed reaction setup as shown in Figure 1. A tubular quartz reactor (ID: 4 mm) placed into a tubular furnace was used as a reactor and the reactor temperature was controlled by a PID controller. For each experiment, 0.1 g of catalyst was loaded into the middle of the reactor with quartz wool before and after the catalytic bed. CO<sub>2</sub>, H<sub>2</sub> (reducing gas), and N<sub>2</sub> (inert gas) were fed into the reactor by a mass flow controller (0–200 sccm) while benzene was introduced by a syringe pump. Gas and liquid streams were mixed in a mixer and introduced to the reactor by a heated line to prevent any condensation. Prior to the catalytic tests, catalysts were reduced in the reactor at 600 °C under H<sub>2</sub> flow (10% H<sub>2</sub> in N<sub>2</sub>) for 1 h. Catalytic dry reforming tests were first conducted at temperatures of 600, 700, and 800 °C with GHSV of 28,000 h<sup>-1</sup> (WHSV = 3.5 g benzene/g catalyst per hour) and benzene concentration of 100 g/m<sup>3</sup> (CO<sub>2</sub>/C<sub>6</sub>H<sub>6</sub> ratio = 6) for both Ni(15 wt.)/ $\gamma$ -Al<sub>2</sub>O<sub>3</sub> and LaCoO<sub>3</sub> catalysts. The effects of CO<sub>2</sub>/C<sub>6</sub>H<sub>6</sub> ratio and flow rate were then tested for the LaCoO<sub>3</sub> catalyst (Table 2). The unreacted benzene at the outlet was collected by a cold trap (i.e. an impinge bottle filled with isopropyl alcohol in a Dewar flask at 0 °C) and the benzene-free gas mixture was sent to a gas chromatography (GC) unit via a 6-way valve with 100- $\mu$ L sampling port. Gas compositions were analyzed by the GC unit (HP 4890A, Agilent Technologies, Santa Clara, CA, USA) equipped with a TCD detector and Carboxen 1010 capillary column (Sigma Aldrich, St. Louis, MO, USA). For clear separation of the peaks of outlet gases (CO, H<sub>2</sub>, CH<sub>4</sub>, CO<sub>2</sub>, and H<sub>2</sub>O), the GC analysis conditions shown in Table 3 were used.



Figure 1. The fixed-bed reaction setup used for dry reforming experiments.

Table 2. Dry reforming test conditions.

Catalysts	Temperature (°C)	CO <sub>2</sub> /C <sub>6</sub> H <sub>6</sub> ratio	GHSV (h <sup>-1</sup> )	WHSV (g benzene/g catalyst per hour)	Benzene concentration (g/m <sup>3</sup> )	Residence time (s)
LaCoO <sub>3</sub> , Ni(15 wt.%)-Al <sub>2</sub> O <sub>3</sub>	600, 700, 800	6	28,000	3.5	100	0.13
LaCoO <sub>3</sub>	800	12	28,000	3.5	100	0.13
LaCoO <sub>3</sub>	800	3	28,000	3.5	100	0.13
LaCoO <sub>3</sub>	800	6	14,000	1.75	100	0.26

Table 3. GC analysis conditions.

Column	Oven temperature	Injection temperature (°C)	Detector temperature (°C)	Amount of gas injection (μL)
Carboxen 1010	35 °C (held for 5 min), heated to 250 °C with a rate of 24 °C/min	200	230	100

For each experiment, the percentage H<sub>2</sub> and CO yields were calculated considering the reaction stoichiometry as follows:

$$Y_{H_2} = \frac{\dot{N}_{H_2}}{3\dot{N}_{C_6H_6, in}} \times 100. \quad (2)$$

$$Y_{CO} = \frac{\dot{N}_{CO}}{6\dot{N}_{C_6H_6, in} + \dot{N}_{CO_2, in}} \times 100. \quad (3)$$

Here,  $\dot{N}$  represents the molar flow rate in mol/min for all considered compounds shown as subscripts with their chemical formulas and the subscript “in” represents the inlet. For all experiments, benzene conversion was assumed to be 100% since no noticeable benzene was detected at the reactor outlet and the high reaction temperature (no kinetic

limitation) and high equilibrium constants of benzene reforming and decomposition reactions (Figure S3) favored complete benzene conversion.

### 3. Results and discussion

#### 3.1. Thermodynamic analysis of benzene dry reforming

Benzene and CO<sub>2</sub> conversions and product molar fractions at equilibrium conditions were determined using the Gibbs free energy minimization method to assess the maximum achievable reactant conversions and product yields. Figure 2 shows the change of equilibrium conversion of benzene and CO<sub>2</sub> and the product molar fractions as a function of temperature between 600 and 900 °C for 3 different CO<sub>2</sub>/C<sub>6</sub>H<sub>6</sub> molar ratios (3, 6, and 12). As seen from the Figure, benzene was completely converted into products for all CO<sub>2</sub>/benzene ratios and temperatures while there was no complete conversion for CO<sub>2</sub> even at the substoichiometric condition (CO<sub>2</sub>/C<sub>6</sub>H<sub>6</sub> = 3) and high temperature. CO<sub>2</sub> conversion increased with temperature for all CO<sub>2</sub>/C<sub>6</sub>H<sub>6</sub> ratios due to the endothermic nature of benzene dry reforming reactions (Table 4 and Figure S3). The maximum CO<sub>2</sub> conversion observed at 900 °C was about 96% for the CO<sub>2</sub>/C<sub>6</sub>H<sub>6</sub> ratios of 3 and 6, while it was 58% for the CO<sub>2</sub>/C<sub>6</sub>H<sub>6</sub> ratio of 12 (excess CO<sub>2</sub> condition). The main equilibrium products were CO, H<sub>2</sub>, carbon, H<sub>2</sub>O, and CH<sub>4</sub>. The change of molar fractions of products including unreacted CO<sub>2</sub> is also seen in Figure 1. That Figure shows that the amount of CO and H<sub>2</sub> increased with temperature, whereas the amount of carbon, H<sub>2</sub>O, and CH<sub>4</sub> decreased along with the unreacted CO<sub>2</sub>. This is mainly associated with endothermic Boudouard, carbon steam reforming, and methane steam reforming reactions (Table 4 and Figure S3). The results indicated that

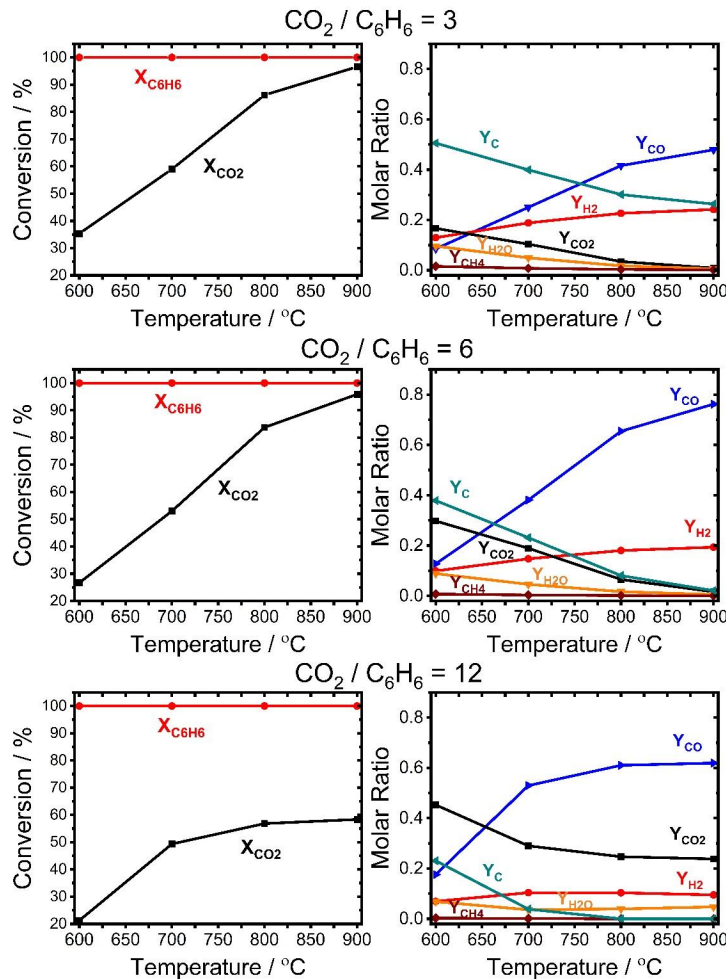


**Figure 2.** Change of benzene and CO<sub>2</sub> conversion and product molar fractions at various temperatures and CO<sub>2</sub>/C<sub>6</sub>H<sub>6</sub> ratios at equilibrium conditions based on Gibbs free energy minimization.

**Table 4.** Possible reactions occurring in the reaction medium.

No	Reaction type	Chemical equation	$\Delta\hat{h}_{rxn}$ (kJ/mol)
1	Boudouard	$C + CO_2 \leftrightarrow CO$	172.4
2	Carbon steam reforming (CSR)	$C + H_2O (g) \leftrightarrow CO + H_2$	131.3
3	Water-gas shift (WGS)	$CO + H_2O (g) \leftrightarrow CO_2 + H_2$	-41.1
4	Benzene dry reforming (BDR-1)	$C_6H_6 + 6CO_2 \leftrightarrow 12CO + 3H_2$	951.6
5	Benzene dry reforming (BDR-2)	$C_6H_6 + 9CO_2 \leftrightarrow 9CO + 3H_2O(g)$	1075.0
6	Benzene decomposition (BD)	$C_6H_6 \leftrightarrow 6C + 3H_2$	-82.9
7	Methane steam reforming (MSR)	$CH_4 + H_2O (g) \leftrightarrow CO + 3H_2$	206.1
8	Methane dry reforming	$CH_4 + CO_2 \leftrightarrow 2CO + 2H_2$	247.0
9	Methanation	$C + H_2 \leftrightarrow CH_4$	-75.0

the chemical equilibrium mainly favored CO, H<sub>2</sub>, carbon, and H<sub>2</sub>O formation and that high temperatures are required to maximize CO and H<sub>2</sub> yield and minimize carbon accumulation.

### 3.2. Catalyst characterization

The crystal structures of both LaCoO<sub>3</sub> and Ni(15 wt.%)/ $\gamma$ -Al<sub>2</sub>O<sub>3</sub> catalysts were analyzed by XRD technique. As seen from Figure 3, the XRD spectra of LaCoO<sub>3</sub> showed the characteristic peaks of hexagonal-rhombohedral LaCoO<sub>3</sub> (ICDD: 75-0249) at 23.26°, 33.13°, 40.88°, 47.56°, 59.19°, and 69.5°, which were assigned to the (100), (110), (111), (200), (211), and (220) planes. This result confirmed that the synthesis of LaCoO<sub>3</sub> was successfully done. For Ni(15 wt.%)/ $\gamma$ -Al<sub>2</sub>O<sub>3</sub> catalyst, the XRD spectra exhibited the presence of  $\gamma$ -Al<sub>2</sub>O<sub>3</sub> (ICDD: 26-0031) and NiO (ICDD: 47-1049) phases as evidenced by their characteristic peaks. The average crystalline sizes of both LaCoO<sub>3</sub> and NiO phases for the related catalysts were also determined from the selected planes and peak positions shown in Table 5 using the Debye-Scherrer formula. The average crystalline sizes of LaCoO<sub>3</sub> and NiO were calculated as 28.8 and 4.4 nm.

The surface area, pore volume, and average pore size of the catalysts were determined using N<sub>2</sub> adsorption-desorption experiments. As seen from Table 6, the BET surface area and pore volume of the LaCoO<sub>3</sub> catalyst were almost 7-fold lower than those of the Ni(15 wt.%)/ $\gamma$ -Al<sub>2</sub>O<sub>3</sub> catalyst while the average pore sizes of both catalysts were similar, which can be explained by the difference in the tortuosity of the catalysts or the difference in the pore shape and structures of the catalysts (Supplementary information, Figure S4).

The reduction and oxidation behaviors of the catalysts were investigated by TPR and TPO analyses (Figure 4). The catalysts were first reduced under the flow of H<sub>2</sub> in Ar (1st TPR), then oxidized under the flow of O<sub>2</sub> in He (TPO) and successively reduced again (2nd TPR) by a TPR/TPO cycle. The first TPR and TPO tests were used to determine the reduction and oxidation behaviors of the catalysts while the second TPR was used to evaluate the reversibility of the catalysts after oxygen exchange. In the first TPR run, the TPR spectra of the LaCoO<sub>3</sub> catalyst showed three reduction peaks at 345, 390, and 560 °C. The first two peaks observed at low temperatures were assigned to the reduction of Co<sup>3+</sup> to Co<sup>2+</sup> (LaCoO<sub>3</sub>+1/2H<sub>2</sub>→LaCoO<sub>2.5</sub>+1/2H<sub>2</sub>O) while the latter was related to the reduction of Co<sup>2+</sup> to the metallic cobalt resulting in La<sub>2</sub>O<sub>3</sub> formation (LaCoO<sub>2.5</sub>+H<sub>2</sub>→1/2La<sub>2</sub>O<sub>3</sub>+Co<sup>0</sup>+H<sub>2</sub>O) [47–50]. The corresponding peak areas of these reduction steps had a 1:1.9 ratio, which is very close to the stoichiometric ratio of 2. The degree of reduction was calculated as 0.75 (Table 7) according to total H<sub>2</sub> consumption for successive reduction steps, suggesting that only 75% of LaCoO<sub>3</sub> was accessible for reduction. The TPR spectra of the Ni(15 wt.%)/ $\gamma$ -Al<sub>2</sub>O<sub>3</sub> catalyst also showed three reduction peaks at 348, 500, and 820 °C with an additional shoulder at a low temperature (435 °C). The peaks at 348 and 500 °C were associated with the reduction of the  $\alpha$ -NiO phase and  $\beta$ -NiO phase (NiO+H<sub>2</sub>→Ni+H<sub>2</sub>O), respectively. The former had a weak interaction with the alumina support while the latter had a strong interaction with the support [51–54]. It is known that the TPR peak temperature shifts to higher temperatures with increasing strength between the support and metal, suggesting that the shoulder at 435 °C can be attributed to the reduction of NiO having an intermediate interaction with the support. In contrast to the others, the broad peak at 820 °C was assigned to the reduction of NiAl<sub>2</sub>O<sub>4</sub> [55–57]. The degree of reduction for the Ni-Al<sub>2</sub>O<sub>3</sub> catalyst was calculated as 60%, indicating that it has lower reducibility compared to the LaCoO<sub>3</sub> catalyst.

After the first TPR run the oxidation characteristics of the catalysts were observed by TPO analysis. The TPO spectra of the LaCoO<sub>3</sub> catalyst showed three oxidation peaks at 285, 640, and 745 °C. The low temperature peak was due to the oxidation of La<sub>2</sub>O<sub>3</sub> to LaCoO<sub>2.5</sub> while the high temperature peaks were assigned to the oxidation of LaCoO<sub>2.5</sub> to LaCoO<sub>3</sub>. A negative peak was also observed in the TPO spectra of the LaCoO<sub>3</sub> catalyst. This can be attributed to the decomposition of Co<sub>3</sub>O<sub>4</sub> by oxygen release (Co<sub>3</sub>O<sub>4</sub> = 3CoO + 1/2O<sub>2</sub>) [58], suggesting that a small amount of Co<sub>3</sub>O<sub>4</sub> also formed during



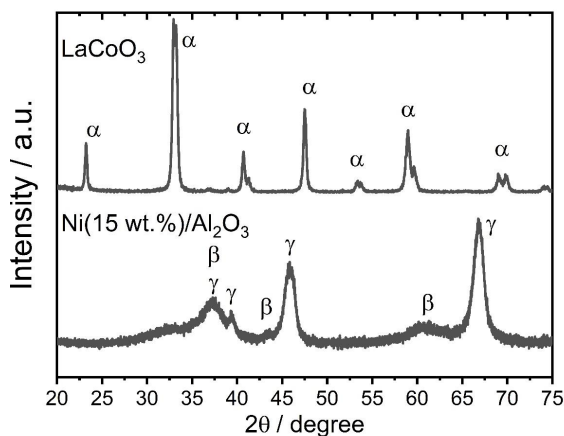


**Figure 3.** XRD spectra of Ni(15 wt.%)/ $\gamma$ - $\text{Al}_2\text{O}_3$  and  $\text{LaCoO}_3$  catalysts.  $\alpha$ ,  $\beta$ , and  $\gamma$  represent  $\text{LaCoO}_3$ , NiO, and  $\gamma$ - $\text{Al}_2\text{O}_3$  phases, respectively.

**Table 5.** Average crystalline sizes of catalysts obtained from XRD spectra.

Catalyst - phase	Facet	Peak position (2q)	Average crystalline size (nm)
Ni(15 wt.%)/ $\gamma$ - $\text{Al}_2\text{O}_3$ - NiO	111	37.26	4.4
$\text{LaCoO}_3$	110	33.13	28.8

**Table 6.** BET surface area, pore volume, and average pore size of catalysts obtained from  $\text{N}_2$  adsorption and desorption experiments.

Catalyst	BET surface area ( $\text{m}^2/\text{g}$ )	Pore volume ( $\text{cm}^3/\text{g}$ )	Average pore size (nm)
Ni(15 wt.%)/ $\gamma$ - $\text{Al}_2\text{O}_3$	43.58	0.035	4.32
$\text{LaCoO}_3$	5.91	0.005	4.33

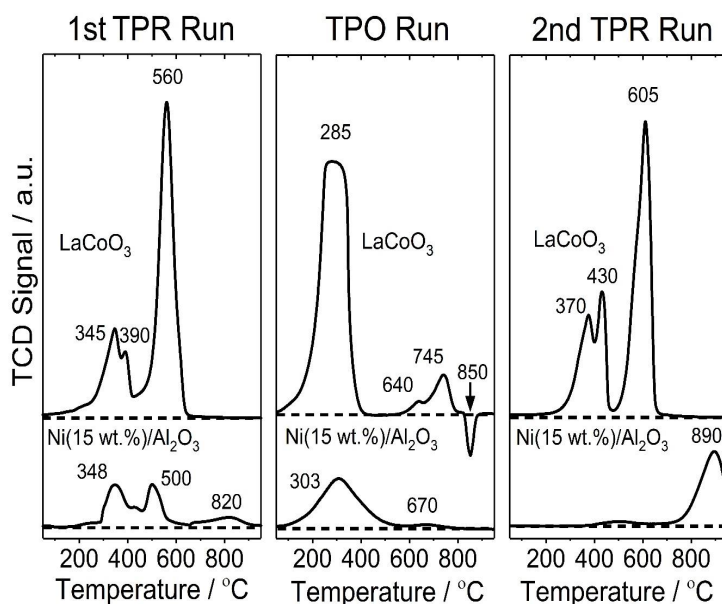


**Figure 4.** Temperature-programmed reduction and oxidation spectra for Ni(15 wt.%)/ $\gamma$ - $\text{Al}_2\text{O}_3$  and  $\text{LaCoO}_3$  catalysts. The heating rate for each run is  $10^\circ\text{C}/\text{min}$ .

**Table 7.** H<sub>2</sub> consumption of catalysts and their degree of reduction obtained from TPR runs.

Catalysts	H <sub>2</sub> consumption (mmol/g)			Degree of reduction	
	1st TPR	2nd TPR*	Theoretical**	1st TPR	2nd TPR
Ni-Al <sub>2</sub> O <sub>3</sub>	1.32	1.47	2.22	0.59	0.66
LaCoO <sub>3</sub>	4.56	4.71	6.10	0.75	0.77

\*: The weight of the catalyst at the beginning of the first TPR run was taken for the calculation.

\*\* : The theoretical H<sub>2</sub> consumptions for the Ni-Al<sub>2</sub>O<sub>3</sub> and LaCoO<sub>3</sub> catalysts were determined based on the stoichiometry of the following reactions: (i) NiO + Al<sub>2</sub>O<sub>3</sub> + H<sub>2</sub> = Ni + Al<sub>2</sub>O<sub>3</sub> + H<sub>2</sub>O; (ii) LaCoO<sub>3</sub> + 3/2 H<sub>2</sub> = 1/2 La<sub>2</sub>O<sub>3</sub> + Co + 3/2 H<sub>2</sub>O.

the oxidation. In contrast to the LaCoO<sub>3</sub> catalyst, the Ni(15 wt.)/γ-Al<sub>2</sub>O<sub>3</sub> catalyst had one strong and one weak oxidation peak at 303 and 670 °C, which were related to the formation of NiAl<sub>2</sub>O<sub>4</sub> and β-NiO phases [59]. These assignments were also verified by the second TPR run, which showed the reduction peaks of the related phases. The second TPR spectra of the Ni(15 wt.)/γ-Al<sub>2</sub>O<sub>3</sub> catalyst showed a significant difference compared to the first one. The peaks associated with the reduction of NiO phases almost disappeared and the intensity of the peak related to the reduction of NiAl<sub>2</sub>O<sub>4</sub> increased prominently. This indicated that metallic nickel was almost completely inserted in the alumina structure after the TPO run. In contrast to the Ni(15 wt.)/γ-Al<sub>2</sub>O<sub>3</sub> catalyst, the reduction peaks in the second TPR run of the LaCoO<sub>3</sub> catalyst were similar to the ones obtained in the first TPR run with a small shift to high temperatures, suggesting that LaCoO<sub>3</sub> had good structural stability upon oxygen exchange.

### 3.3. Dry reforming activity

Dry reforming experiments were performed under the conditions specified in Table 2 for the LaCoO<sub>3</sub> and Ni(15 wt.)/γ-Al<sub>2</sub>O<sub>3</sub> catalysts. Changes of CO<sub>2</sub> conversion and H<sub>2</sub>/C<sub>6</sub>H<sub>6,in</sub> and CO/CO<sub>2,reacted</sub> ratios as a function of time at 600, 700, and 800 °C are shown in Figure 5. As seen from the Figure, a steady response was obtained for all experiments after the first 2 or 3 data points (approximately 50 min). The unsteady behavior in CO<sub>2</sub> conversion and H<sub>2</sub>/C<sub>6</sub>H<sub>6,in</sub> and CO/CO<sub>2,reacted</sub> ratios in the period of interest was attributed to the limited gas passage through the reactor due to pressure build-up, which was removed at the end of this period (Supplementary information, Figure S5). The CO<sub>2</sub> conversion and H<sub>2</sub>/C<sub>6</sub>H<sub>6,in</sub> and CO/CO<sub>2,reacted</sub> ratios obtained at the end of this period (at 50 min) were taken as initial values and average values were calculated based on those initial values and the final values recorded at the end of the experiments. The results are tabulated in Table 8. Equilibrium CO<sub>2</sub> conversion and H<sub>2</sub>/C<sub>6</sub>H<sub>6,in</sub> and CO/CO<sub>2,reacted</sub> ratios were also found based on Gibbs free energy minimization (see subsection 3.1 and Figure S6) and are listed in Table 9 to allow an evaluation of the results in comparison to equilibrium conditions. The reaction results indicated that at both 700 and 800 °C the LaCoO<sub>3</sub> catalyst had a higher CO<sub>2</sub> conversion and H<sub>2</sub>/C<sub>6</sub>H<sub>6,in</sub> ratio than the Ni(15 wt.)/γ-Al<sub>2</sub>O<sub>3</sub> catalyst, while it had a lower CO/CO<sub>2,reacted</sub> ratio compared to its counterpart. At 800 °C the equilibrium CO<sub>2</sub> conversion was almost achieved (80.1%) for the LaCoO<sub>3</sub> catalyst while the CO<sub>2</sub> conversion of the Ni(15 wt.)/γ-Al<sub>2</sub>O<sub>3</sub> catalyst was 62.7%. At 800 °C the H<sub>2</sub>/C<sub>6</sub>H<sub>6,in</sub> and CO/CO<sub>2,reacted</sub> ratios observed for the LaCoO<sub>3</sub> catalyst at the end of the experiment were 2.45 and 1.97, respectively. The corresponding H<sub>2</sub> and CO yields were 81.8% and 78.4%, respectively, indicating that benzene dry reforming primarily results in H<sub>2</sub> and CO formation. The H<sub>2</sub> and CO yields for the Ni(15 wt.)/γ-Al<sub>2</sub>O<sub>3</sub> catalyst were 65.0 and 67.9, respectively, suggesting that the LaCoO<sub>3</sub> catalyst outperformed the Ni(15 wt.)/γ-Al<sub>2</sub>O<sub>3</sub> catalyst in terms of H<sub>2</sub> and CO production. For both catalysts, the CO<sub>2</sub> conversion and H<sub>2</sub>/C<sub>6</sub>H<sub>6,in</sub> and CO/CO<sub>2,reacted</sub> ratios obtained at 800 °C showed a steady decline associated with gas disruption due to carbon accumulation in the reactor. The carbon formation on the catalyst surface was confirmed by TGA analysis of the used catalysts (Supplementary information, Figures S7–S9). The gas disruption due to carbon accumulation was less prominent for the results obtained at 700 and 600 °C, but it still caused a small deviation from the steady response due to the resulting uneven gas distribution at the sampling port. This may explain why the average CO<sub>2</sub> conversions and CO yields of the LaCoO<sub>3</sub> catalyst were higher than the related equilibrium conversions and yields at 700 and 600 °C (Table 9) to an extent beyond the specified uncertainties (e.g., at 600 °C 32.8 vs. 26.7, with ±5% uncertainty), which only accounted for instrumental and calibration errors. Although the relevant data are beyond the error margin by a small difference, it is still possible to infer that the LaCoO<sub>3</sub> catalyst has CO<sub>2</sub> conversion and CO yield very close to equilibrium values and higher than those for the Ni(15 wt.)/γ-Al<sub>2</sub>O<sub>3</sub> catalyst. The effects of temperature on CO<sub>2</sub> conversion and CO and H<sub>2</sub> yields were also clearly seen in the results. There was a significant decrease in conversion and yields with decreasing temperature for both catalysts. This was attributed to the strong endothermicity of dry reforming reactions (Table 4 and Figure S3).

One of the important considerations regarding the results is the difference in the experimental time for each test. This is related to the reactor blockage caused by carbon build-up. When the gas flow was significantly disrupted, the operation was discontinued. For that reason, no reliable data were obtained for the Ni(15 wt.)/γ-Al<sub>2</sub>O<sub>3</sub> catalyst at 600 °C and such

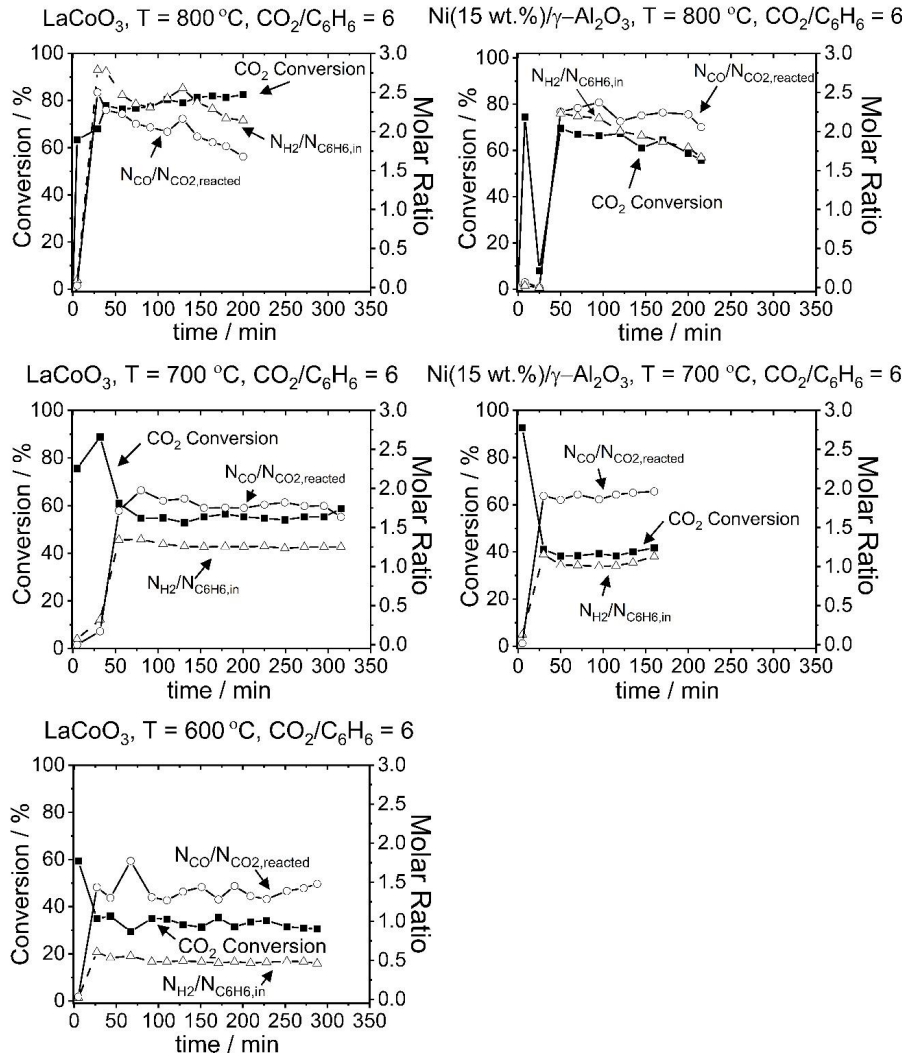


Figure 5. Change of CO<sub>2</sub> conversion and H<sub>2</sub>/C<sub>6</sub>H<sub>6,in</sub> and CO/CO<sub>2,reacted</sub> ratios as a function of time for LaCoO<sub>3</sub> and Ni(15 wt.)/γ-Al<sub>2</sub>O<sub>3</sub> catalysts at 600, 700, and 800 °C and at the CO<sub>2</sub>/C<sub>6</sub>H<sub>6</sub> ratio of 6.

Table 8. Average values of CO<sub>2</sub> conversion, H<sub>2</sub> and CO yields, and H<sub>2</sub>/C<sub>6</sub>H<sub>6,in</sub> and CO/CO<sub>2,reacted</sub> ratios obtained for LaCoO<sub>3</sub> and Ni(15 wt.)/γ-Al<sub>2</sub>O<sub>3</sub> catalysts at different temperatures, N<sub>CO<sub>2</sub></sub>/N<sub>C<sub>6</sub>H<sub>6</sub></sub> ratios, and GHSV (h<sup>-1</sup>). The uncertainties of conversion and yield values are ±5% while the uncertainties of ratios are ±0.2.

Reaction conditions	LaCoO <sub>3</sub>					Ni(15 wt.)/γ-Al <sub>2</sub> O <sub>3</sub>				
	X <sub>CO<sub>2</sub></sub>	N <sub>H<sub>2</sub></sub> /N <sub>C<sub>6</sub>H<sub>6</sub></sub>	Y <sub>H<sub>2</sub></sub> (%)	N <sub>CO</sub> /N <sub>CO<sub>2</sub></sub>	Y <sub>CO</sub>	X <sub>CO<sub>2</sub></sub>	N <sub>H<sub>2</sub></sub> /N <sub>C<sub>6</sub>H<sub>6</sub></sub>	Y <sub>H<sub>2</sub></sub> (%)	N <sub>CO</sub> /N <sub>CO<sub>2</sub></sub>	Y <sub>CO</sub> (%)
600 °C, N <sub>CO<sub>2</sub></sub> /N <sub>C<sub>6</sub>H<sub>6</sub></sub> = 6, 28,000 h <sup>-1</sup>	32.8	0.53	17.8	1.46	23.7	NA				
700 °C, N <sub>CO<sub>2</sub></sub> /N <sub>C<sub>6</sub>H<sub>6</sub></sub> = 6, 28,000 h <sup>-1</sup>	59.8	1.29	43.2	1.67	49.8	41.3	1.14	38.0	1.93	40.0
800 °C, N <sub>CO<sub>2</sub></sub> /N <sub>C<sub>6</sub>H<sub>6</sub></sub> = 6, 28,000 h <sup>-1</sup>	80.1	2.45	81.8	1.97	78.4	62.7	1.95	65.0	2.15	67.9
800 °C, N <sub>CO<sub>2</sub></sub> /N <sub>C<sub>6</sub>H<sub>6</sub></sub> = 12, 28,000 h <sup>-1</sup>	59.8	2.09	69.9	1.82	72.7	NA				
800 °C, N <sub>CO<sub>2</sub></sub> /N <sub>C<sub>6</sub>H<sub>6</sub></sub> = 3, 28,000 h <sup>-1</sup>	73.5	1.72	57.2	1.54	38.7	NA				
800 °C, N <sub>CO<sub>2</sub></sub> /N <sub>C<sub>6</sub>H<sub>6</sub></sub> = 6, 14,000 h <sup>-1</sup>	72.7	2.37	78.9	2.21	78.1	NA				

**Table 9.** Equilibrium CO<sub>2</sub> conversion, H<sub>2</sub> and CO yields, and H<sub>2,in</sub>/C<sub>6H<sub>6,in</sub></sub> and CO<sub>in</sub>/CO<sub>2,reacted</sub> ratios at different temperatures and N<sub>CO<sub>2</sub></sub>/N<sub>C<sub>6H<sub>6</sub></sub></sub> ratios.

Reaction conditions	X <sub>CO<sub>2</sub></sub>	N <sub>H<sub>2</sub></sub> /N <sub>C<sub>6H<sub>6</sub></sub></sub>	Y <sub>H<sub>2</sub></sub> (%)	N <sub>CO</sub> /N <sub>CO<sub>2</sub></sub>	Y <sub>CO</sub> (%)
600 °C, N <sub>CO<sub>2</sub></sub> /N <sub>C<sub>6H<sub>6</sub></sub></sub> = 6	26.7	1.47	49.0	1.18	15.7
700 °C, N <sub>CO<sub>2</sub></sub> /N <sub>C<sub>6H<sub>6</sub></sub></sub> = 6	53.0	2.20	73.3	1.79	47.3
800 °C, N <sub>CO<sub>2</sub></sub> /N <sub>C<sub>6H<sub>6</sub></sub></sub> = 6	83.7	2.70	90.0	1.95	81.6
800 °C, N <sub>CO<sub>2</sub></sub> /N <sub>C<sub>6H<sub>6</sub></sub></sub> = 12	56.8	2.17	72.3	1.88	71.1
800 °C, N <sub>CO<sub>2</sub></sub> /N <sub>C<sub>6H<sub>6</sub></sub></sub> = 3	86.2	2.70	90.0	1.92	55.1

data are not presented here. The absence of experimental data at 600 °C and a lower experimental time (160 min) at 700 °C for the Ni(15 wt.)/γ-Al<sub>2</sub>O<sub>3</sub> catalyst in comparison to the LaCoO<sub>3</sub> catalyst (288 min for 600 °C and 315 min for 700 °C) suggested that the LaCoO<sub>3</sub> catalyst showed higher stability than the Ni(15 wt.)/γ-Al<sub>2</sub>O<sub>3</sub> catalyst.

The effects of CO<sub>2</sub>/C<sub>6H<sub>6</sub></sub> ratio and flow rate on conversion and yields were also studied for the LaCoO<sub>3</sub> catalyst. Figure 6 shows the change of CO<sub>2</sub> conversion values and H<sub>2</sub>/C<sub>6H<sub>6,in</sub></sub> and CO/CO<sub>2,reacted</sub> ratios as a function of time at 800 °C and three different CO<sub>2</sub>/C<sub>6H<sub>6</sub></sub> ratios (3, 6, and 12). As seen from the Figure, a lower CO<sub>2</sub> conversion and H<sub>2</sub>/C<sub>6H<sub>6,in</sub></sub> ratio were observed at the CO<sub>2</sub>/C<sub>6H<sub>6</sub></sub> ratio of 12 compared to the experiment conducted at CO<sub>2</sub>/C<sub>6H<sub>6</sub></sub> of 6, whereas CO<sub>in</sub>/CO<sub>2,reacted</sub> remained almost constant on average. The relatively low CO<sub>2</sub> conversion can be explained by the presence of excess CO<sub>2</sub> while the low H<sub>2,in</sub>/C<sub>6H<sub>6,in</sub></sub> ratio and the similar CO<sub>in</sub>/CO<sub>2,reacted</sub> values were attributed to the differences in the reaction occurring under related conditions. At the CO<sub>2</sub>/C<sub>6H<sub>6</sub></sub> ratio of 6, stoichiometric benzene dry reforming (BDR-1 in Table 4) mainly occurred, whereas with excess CO<sub>2</sub> a dry reforming reaction with a stoichiometry ratio of 9 CO<sub>2</sub>/C<sub>6H<sub>6</sub></sub> (BDR-2 in Table 4) and carbon steam reforming reaction (CSR in Table 4) occurred as well. The dry reforming reaction with a stoichiometry ratio of 9 led to a decrease in H<sub>2</sub> yield while the carbon steam reforming reaction promoted CO formation and maintained the CO yield. A lower CO<sub>2</sub> conversion and H<sub>2</sub> yield were also observed under substoichiometric conditions (CO<sub>2</sub>/C<sub>6H<sub>6</sub></sub> = 3), accompanied by a lower CO yield. This was attributed to carbon deposition. For this reason, a single data point was obtained for this condition. The effect of flow rate was also tested under stoichiometric conditions by decreasing the flow rate by 2-fold. No prominent change was observed compared to the high flow rate condition, suggesting that external mass transfer resistance was not effective in the relevant flow rate range (14,000–28,000 h<sup>-1</sup>).

The dry reforming results showed that the LaCoO<sub>3</sub> catalyst had higher CO<sub>2</sub> conversion and CO and H<sub>2</sub> yields compared to the reference Ni(15 wt.)/γ-Al<sub>2</sub>O<sub>3</sub> catalyst. This could be linked to the high oxygen exchange capacity of the LaCoO<sub>3</sub> catalyst. Prior to the dry reforming experiment, catalyst reduction at 600 °C under H<sub>2</sub> environment resulted in Co and La<sub>2</sub>O<sub>3</sub> formation for the LaCoO<sub>3</sub> catalyst, while it yielded Ni and Al<sub>2</sub>O<sub>3</sub> for the Ni(15 wt.)/γ-Al<sub>2</sub>O<sub>3</sub> catalyst as seen from the TPR analysis. It is known from the literature that benzene adsorbs on metal surfaces via its two atoms, and it subsequently decomposes to C<sub>x</sub>H<sub>y</sub> carbon, and H<sub>2</sub> via C-C and C-H bond scissions [28,60], which occurs on metal sites of both catalyst surfaces (Rxn 1–3 in Table 10). However, the catalysts differed from each other in terms of the reactions between CO<sub>2</sub> and catalyst surfaces. On the LaCoO<sub>3</sub> surface, Co and La<sub>2</sub>O<sub>3</sub> reacted with CO<sub>2</sub> to form CO and LaCoO<sub>3</sub> (Rxn 4, Table 10) [35,37,61] or La<sub>2</sub>O<sub>3</sub> reacted with CO<sub>2</sub> to form La<sub>2</sub>O<sub>2</sub>CO<sub>3</sub> (Rxn 5, Table 10) [62,63] with the exchange of the lattice oxygen. The resulting species further reacted with C<sub>x</sub>H<sub>y</sub> species, surface hydrogen, and surface carbon to produce CO, H<sub>2</sub>, and H<sub>2</sub>O (Rxn 6–11). These reaction steps were less likely to happen on the Ni(15 wt.)/γ-Al<sub>2</sub>O<sub>3</sub> surface, where CO<sub>2</sub> directly reacted with surface moieties (C<sub>x</sub>H<sub>y</sub> species, surface carbon) to produce CO and H<sub>2</sub>O (Rxn 12–13). The faster kinetics of the surface CO<sub>2</sub> reaction and the following oxidation of surface species on the LaCoO<sub>3</sub> catalyst led to higher CO<sub>2</sub> conversion and product yields compared to its counterpart due to its high oxygen exchange capability as seen from TPR analysis (see subsection 3.2). The presumed reaction schemes for both catalysts are shown in Figure 7.

The performance of the LaCoO<sub>3</sub> was evaluated in comparison to the conventional Ni-Al<sub>2</sub>O<sub>3</sub> catalyst for benzene dry reforming, which mimics catalytic tar conversion. The results indicated that the LaCoO<sub>3</sub> catalyst outperformed the Ni-Al<sub>2</sub>O<sub>3</sub> catalyst in terms of CO<sub>2</sub> conversion and CO and H<sub>2</sub> yields. For all temperatures studied (600, 700, and 800 °C), the LaCoO<sub>3</sub> catalyst showed about 18% greater CO<sub>2</sub> conversion and approximately 5%–17% higher H<sub>2</sub> and CO yields than the Ni-Al<sub>2</sub>O<sub>3</sub> catalyst. The benzene dry reforming activity of the LaCoO<sub>3</sub> catalyst was also found to be better than that of other catalysts tested in the literature, such as dolomite (CaO.MgO) [28] and NiFe/SiC [23]. For the dolomite catalyst, 33% benzene conversion was reported at 800 °C and stoichiometric CO<sub>2</sub> conditions, which is much lower than the benzene conversion for the LaCoO<sub>3</sub> catalyst in the present study under similar conditions (800 °C, CO<sub>2</sub>/C<sub>6H<sub>6</sub></sub> = 12) considering that the H<sub>2</sub> yield was 67.5% (corresponding to at least 67.5% benzene conversion if benzene is assumed to convert only to H<sub>2</sub>). Similarly, the H<sub>2</sub> and CO yields observed on the NiFe/SiC catalyst at 840 °C under excess CO<sub>2</sub> were 7.2% and 20%,

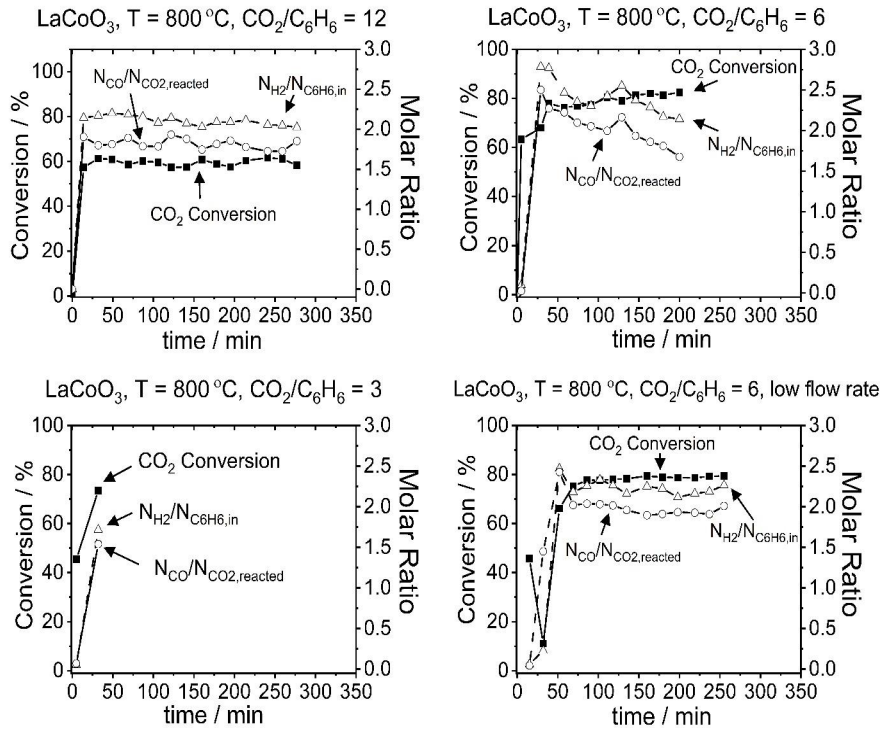


**Figure 6.** CO<sub>2</sub> conversion and H<sub>2</sub>/C<sub>6</sub>H<sub>6,in</sub> and CO/CO<sub>2,reacted</sub> ratios obtained for the LaCoO<sub>3</sub> catalyst at 800 °C and at the CO<sub>2</sub>/C<sub>6</sub>H<sub>6</sub> ratio of 12 (top left), 6 (top right), and 3 (bottom left) and at a low flow rate (bottom right).

**Table 10.** Presumed reaction steps occurring on catalyst surfaces.

No.	Reaction*	Catalysts
1	$C_6H_6 + M = M-C_6H_6$	LaCoO <sub>3</sub> , Ni(15 wt.%)/γ-Al <sub>2</sub> O <sub>3</sub> M: Co, Ni
2	$M-C_6H_6 = M-C_xH_y + M-zC + (6-y)/2 H_2$	
3	$M-C_xH_y = M-xC + y/2 H_2$ (or +M-yH)	
4	$3/2 CO_2 + 1/2 La_2O_3 + Co = 3/2 CO + LaCoO_3$	LaCoO <sub>3</sub>
5	$CO_2 + La_2O_3 = La_2O_2CO_3$	
6	$LaCoO_3 + Co-C_xH_y = zCO + y/2 H_2 + 1/2 La_2O_3 + 2Co$	
7	$LaCoO_3 + 3/2 Co-C = 3/2 CO + 1/2 La_2O_3 + Co$	
8	$LaCoO_3 + 3 Co-H = 3/2 H_2O + 1/2 La_2O_3 + Co$	
9	$La_2O_2CO_3 + Co-C_xH_y = zCO + y/2 H_2 + La_2O_3$	
10	$La_2O_2CO_3 + Co-C = 2CO + La_2O_3$	
11	$La_2O_2CO_3 + 2Co-H = H_2O + CO + La_2O_3$	Ni(15 wt.%)/γ-Al <sub>2</sub> O <sub>3</sub>
12	$Ni-C_xH_y + Al_2O_3-CO_2 = (2-y)/2CO + y/2 H_2O + Ni + Al_2O_3$	
13	$Ni-C + Al_2O_3-CO_2 = 2CO + Ni + Al_2O_3$	

\*: x, y, and z represent stoichiometric coefficients.

respectively. Under similar conditions (800 °C, CO<sub>2</sub>/C<sub>6</sub>H<sub>6</sub> = 12), the H<sub>2</sub> and CO yields were 69.9% and 72.7% for the LaCoO<sub>3</sub> catalyst. These findings suggest that the LaCoO<sub>3</sub> catalyst is a promising catalyst candidate for catalytic tar removal and CO<sub>2</sub> valorization as evidenced by its relatively high activity towards benzene dry reforming.

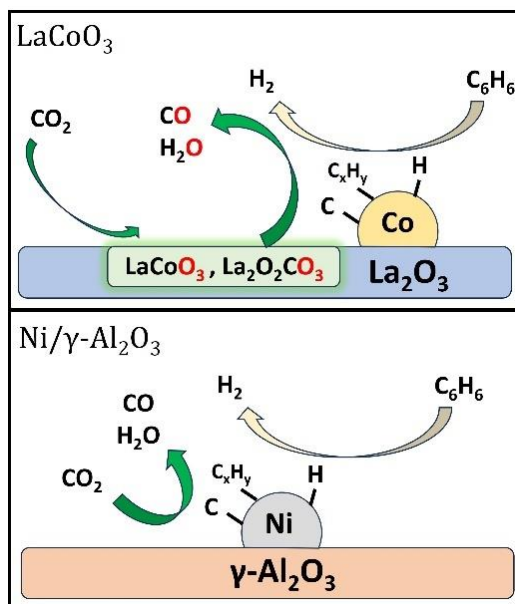


**Figure 7.** Presumed reaction schemes for benzene dry reforming on the LaCoO<sub>3</sub> (top) and Ni/ $\gamma$ -Al<sub>2</sub>O<sub>3</sub> (bottom) catalysts.

#### 4. Conclusion

Benzene dry reforming provides valuable information for the catalytic cracking of tar used as a posttreatment unit in biomass gasification. In this study, benzene was taken as a model molecule for tar compounds due to its high thermal stability and abundance at the outlet of biomass gasifiers while LaCoO<sub>3</sub> was selected as the dry reforming catalyst to overcome the challenges observed for conventional Ni-Al<sub>2</sub>O<sub>3</sub> catalysts (e.g., coke deposition, low stability). Catalyst characterization was performed to determine the crystal structure, surface area, and reduction/oxidation behavior of the catalyst, which helped in determining the structure–activity relationship. Dry reforming activity tests of the LaCoO<sub>3</sub> catalyst were conducted at three different temperatures (600, 700, and 800 °C) and CO<sub>2</sub>/C<sub>6</sub>H<sub>6</sub> ratios (3, 6, and 12) and two different space velocities (14,000 and 28,000 h<sup>-1</sup>) and compared to the Ni(15 wt.%)/ $\gamma$ -Al<sub>2</sub>O<sub>3</sub> catalyst. The results showed that the LaCoO<sub>3</sub> catalyst achieved 18% higher CO<sub>2</sub> conversion, 5%–17% higher H<sub>2</sub> yield, 10% higher CO yield, and better stability than the Ni(15 wt.%)/ $\gamma$ -Al<sub>2</sub>O<sub>3</sub> catalyst. The difference in reactivity was linked to the high oxygen exchange ability of the LaCoO<sub>3</sub> catalyst, which promotes the oxidation of carbon and other surface species by lattice oxygen transfer, leading to higher CO<sub>2</sub> conversion and CO and H<sub>2</sub> yields.

#### Acknowledgments

This research was financially supported by the Scientific and Technological Research Council of Türkiye within the scope of Scientific Research Program 2232 - Return to Country Research Fellowship Program, under the project number and title of “115C027 - Catalytic Tar Removal from the Gasifier Outlet.” The authors gratefully acknowledge Dr. Atalay Çalışan and Veysi Halvacı from Middle East Technical University’s Chemical Engineering Department for their assistance in the characterization of the material by TPR and in activity tests.

#### References

- [1] Vennestrom PNR, Osmundsen CM, Christensen CH, Taarning E. Beyond petrochemicals: the renewable chemicals industry. *Angewandte Chemie-International Edition* 2011; 50: 10502-10509. <https://doi.org/10.1002/anie.201102117>
- [2] Alonso DM, Bond JQ, Dumesic JA. Catalytic conversion of biomass to biofuels. *Green Chemistry* 2010; 12: 1493-1513. <https://doi.org/10.1039/c004654j>

- [3] Davda RR, Shabaker JW, Huber GW, Cortright RD, Dumesic JA. A review of catalytic issues and process conditions for renewable hydrogen and alkanes by aqueous-phase reforming of oxygenated hydrocarbons over supported metal catalysts. *Applied Catalysis B: Environmental* 2005; 56: 171-186. <https://doi.org/10.1016/J.APCATB.2004.04.027>
- [4] Christensen CH, Rass-Hansen J, Marsden CC, Taarning E, Egeblad K. The renewable chemicals industry. *ChemSusChem* 2008; 1 (4): 283-289. <https://doi.org/10.1002/cssc.200700168>
- [5] Corma A, Iborra S, Velty A. Chemical routes for the transformation of biomass into chemicals. *Chemical Reviews* 2007; 107 (6): 2411-2502. <https://doi.org/10.1021/cr050989d>
- [6] Li C, Zhao X, Wang A, Huber GW, Zhang T. Catalytic transformation of lignin for the production of chemicals and fuels. *Chemical Reviews* 2015; 115: 11559-11624. <https://doi.org/10.1021/acs.chemrev.5b00155>
- [7] Dayton D. A Review of the Literature on Catalytic Biomass Tar Destruction: Milestone Completion Report. National Renewable Energy Laboratory, NREL/TP-510-32815. Golden, CO, USA: National Renewable Energy Laboratory, 2002. <https://doi.org/10.2172/15002876>
- [8] Li C, Suzuki K. Tar property, analysis, reforming mechanism and model for biomass gasification—an overview. *Renewable and Sustainable Energy Reviews* 2009; 13 (3): 594-604. <https://doi.org/10.1016/j.rser.2008.01.009>
- [9] Guan G, Kaewpanha M, Hao X, Abudula A. Catalytic steam reforming of biomass tar: prospects and challenges. *Renewable and Sustainable Energy Reviews* 2016; 58: 450-461. <https://doi.org/10.1016/j.rser.2015.12.316>
- [10] Ammendola P, Lisi L, Ruoppolo G. Development of a honeycomb catalyst based on Rh-LaCoO<sub>3</sub> for conversion of tar into syngas. *Chemical Engineering Transactions* 2015; 43: 553-558. <https://doi.org/10.3303/CET1543093>
- [11] Kong M, Fei J, Wang S, Lu W, Zheng X. Influence of supports on catalytic behavior of nickel catalysts in carbon dioxide reforming of toluene as a model compound of tar from biomass gasification. *Bioresource Technology* 2011; 102 (2): 2004-2008. <https://doi.org/10.1016/j.biortech.2010.09.054>
- [12] Gai C, Dong Y, Yang S, Zhang Z, Liang J et al. Thermal decomposition kinetics of light polycyclic aromatic hydrocarbons as surrogate biomass tar. *RSC Advances* 2016; 6: 83154-83162. <https://doi.org/10.1039/C6RA15513H>
- [13] Han J, Kim H. The reduction and control technology of tar during biomass gasification/pyrolysis: an overview. *Renewable and Sustainable Energy Reviews* 2008; 12 (2): 397-416. <https://doi.org/10.1016/j.rser.2006.07.015>
- [14] Milne TA, Evans RJ, Abatzoglou N. Biomass Gasifier “Tars”: Their Nature, Formation, and Conversion. National Renewable Energy Laboratory, NREL/TP-570-25357. Golden, CO, USA: National Renewable Energy Laboratory, 1998. <https://doi.org/10.2172/3726>
- [15] Huang Z, Wang Y, Dong N, Song D, Lin Y et al. In situ removal of benzene as a biomass tar model compound employing hematite oxygen carrier. *Catalysts* 2022; 12: 1088. <https://doi.org/10.3390/CATAL12101088>
- [16] Lin Y, Liao Y, Yu Z, Fang S, Ma X. A study on co-pyrolysis of bagasse and sewage sludge using TG-FTIR and Py-GC/MS. *Energy Conversion and Management* 2017; 151: 190-198. <https://doi.org/10.1016/J.ENCONMAN.2017.08.062>
- [17] Simell PA, Hirvensalo EK, Smolander VT, Krause AOI. Steam reforming of gasification gas tar over dolomite with benzene as a model compound. *Industrial & Engineering Chemistry Research* 1999; 38: 1250-1257. <https://doi.org/10.1021/ie980646o>
- [18] Yang X, Xu S, Chen Z, Liu J. Improved nickel-olivine catalysts with high coking resistance and regeneration ability for the steam reforming of benzene. *Reaction Kinetics, Mechanisms and Catalysis* 2013; 108: 459-472. <https://doi.org/10.1007/s11144-012-0527-0>
- [19] Bangala DN, Abatzoglou N, Martin JP, Chornet E. Catalytic gas conditioning: application to biomass and waste gasification. *Industrial & Engineering Chemistry Research* 1997; 36 (10): 4184-4192. <https://doi.org/10.1021/ie960785a>
- [20] Claude V, Courson C, Köhler M, Lambert SD. Overview and essentials of biomass gasification technologies and their catalytic cleaning methods. *Energy and Fuels* 2016; 30 (11): 8791-8814. <https://doi.org/10.1021/acs.energyfuels.6b01642>
- [21] Kong M, Fei J, Wang S, Lu W, Zheng X. Influence of supports on catalytic behavior of nickel catalysts in carbon dioxide reforming of toluene as a model compound of tar from biomass gasification. *Bioresource Technology* 2011; 102 (2): 2004-2008. <https://doi.org/10.1016/j.biortech.2010.09.054>
- [22] Laosiripojana N, Sutthisripok W, Charojrochkul S, Assabumrungrat S. Development of Ni-Fe bimetallic based catalysts for biomass tar cracking/reforming: effects of catalyst support and co-fed reactants on tar conversion characteristics. *Fuel Processing Technology* 2014; 127: 26-32. <https://doi.org/10.1016/j.fuproc.2014.06.015>
- [23] Nam H, Wang Z, Shanmugam SR, Adhikari S, Abdoulmoumine N. Chemical looping dry reforming of benzene as a gasification tar model compound with Ni- and Fe-based oxygen carriers in a fluidized bed reactor. *International Journal of Hydrogen Energy* 2018; 43 (41): 18790-18800. <https://doi.org/10.1016/J.IJHYDENE.2018.08.103>
- [24] Abou Rached J, Cesario MR, Estephane J, Tidahy HL, Gennequin C et al. Effects of cerium and lanthanum on Ni-based catalysts for CO<sub>2</sub> reforming of toluene. *Journal of Environmental Chemical Engineering* 2018; 6 (4): 4743-4754. <https://doi.org/10.1016/J.JECE.2018.06.054>

- [25] Dernaika B, Uner D. A simplified approach to determine the activation energies of uncatalyzed and catalyzed combustion of soot. *Applied Catalysis B: Environmental* 2003; 40: 219-229. [https://doi.org/10.1016/S0926-3373\(02\)00152-2](https://doi.org/10.1016/S0926-3373(02)00152-2)
- [26] Chueh WC, Falter C, Abbott M, Scipio D, Furler P et al. High-flux solar-driven thermochemical dissociation of CO<sub>2</sub> and H<sub>2</sub>O using nonstoichiometric ceria. *Science* 2010; 330: 1797-1801. <https://doi.org/10.1126/SCIENCE.1197834>
- [27] Kaya D, Singh D, Kincal S, Uner D. Facilitating role of Pd for hydrogen, oxygen and water adsorption/desorption processes from bulk CeO<sub>2</sub> and CeO<sub>2</sub>/γ-Al<sub>2</sub>O<sub>3</sub>. *Catalysis Today* 2019; 323: 141-147. <https://doi.org/10.1016/J.CATTOD.2018.04.063>
- [28] Simell PA, Hakala NAK, Haario HE, Krause AOI. Catalytic decomposition of gasification gas tar with benzene as the model compound. *Industrial & Engineering Chemistry Research* 1997; 36 (1): 42-51. <https://doi.org/10.1021/ie960323x>
- [29] Devi L, Ptasinski KJ, Janssen FJJG. Pretreated olivine as tar removal catalyst for biomass gasifiers: investigation using naphthalene as model biomass tar. *Fuel Processing Technology* 2005; 86 (6): 707-730. <https://doi.org/10.1016/J.FUPROC.2004.07.001>
- [30] Li L, Meng B, Qin X, Yang Z, Chen J et al. Toluene microwave cracking and reforming over bio-char with in-situ activation and ex-situ impregnation of metal. *Renewable Energy* 2020; 149: 1205-1213. <https://doi.org/10.1016/J.RENENE.2019.10.115>
- [31] Ammendola P, Lisi L, Piriou B, Ruoppolo G. Rh-perovskite catalysts for conversion of tar from biomass pyrolysis. *Chemical Engineering Journal* 2009; 154 (1-3): 361-368. <https://doi.org/10.1016/j.cej.2009.04.010>
- [32] Ammendola P, Cammisa E, Chirone R, Lisi L, Ruoppolo G. Effect of sulphur on the performance of Rh-LaCoO<sub>3</sub> based catalyst for tar conversion to syngas. *Applied Catalysis B: Environmental* 2012; 113-114: 11-18. <https://doi.org/10.1016/j.apcatb.2011.07.024>
- [33] Ammendola P, Cammisa E, Lisi L, Ruoppolo G. Thermochemical stability of alumina-supported Rh-LaCoO<sub>3</sub> catalysts for tar conversion. *Industrial & Engineering Chemistry Research* 2012; 51 (22): 7475-7481. <https://doi.org/10.1021/ie2016448>
- [34] Ammendola P, Chirone R, Lisi L, Piriou B, Russo G. Investigation of the catalytic activity of Rh-LaCoO<sub>3</sub> catalyst in the conversion of tar from biomass devolatilization products. *Applied Catalysis A: General* 2010; 385 (1-2): 123-129. <https://doi.org/10.1016/j.apcata.2010.07.003>
- [35] Zeng R, Jin G, He D, Zhang L, Chen D et al. Oxygen vacancy promoted CO<sub>2</sub> activation over acidic-treated LaCoO<sub>3</sub> for dry reforming of propane. *Materials Today Sustainability* 2022; 19: 100162. <https://doi.org/10.1016/J.MTSUST.2022.100162>
- [36] Lim HS, Lee M, Kim Y, Kang D, Lee JW. Low-temperature CO<sub>2</sub> hydrogenation to CO on Ni-incorporated LaCoO<sub>3</sub> perovskite catalysts. *International Journal of Hydrogen Energy* 2021; 46 (29): 15497-15506. <https://doi.org/10.1016/J.IJHYDENE.2021.02.085>
- [37] Pomiro FJ, Fouga GG, Bohé AE, De Micco G. CO<sub>2</sub> conversion to CO by LaCo<sub>1-x</sub>Fe<sub>x</sub>O<sub>3</sub> (x = 0, 0.25, 0.5, 0.75, 1) perovskite phases at low temperature. *Journal of Alloys and Compounds* 2023; 938: 168671. <https://doi.org/10.1016/J.JALLCOM.2022.168671>
- [38] Hepola J, Simell P. Sulphur poisoning of nickel-based hot gas cleaning catalysts in synthetic gasification gas: I. Effect of different process parameters. *Applied Catalysis B: Environmental* 1997; 14 (3-4): 287-303. [https://doi.org/10.1016/S0926-3373\(97\)00031-3](https://doi.org/10.1016/S0926-3373(97)00031-3)
- [39] Narváez I, Corella J, Orío A. Fresh tar (from a biomass gasifier) elimination over a commercial steam-reforming catalyst. Kinetics and effect of different variables of operation. *Industrial & Engineering Chemistry Research* 1997; 36 (2): 317-327. <https://doi.org/10.1021/ie960235c>
- [40] Caballero MA, Corella J, Aznar MP, Gil J. Biomass gasification with air in fluidized bed. Hot gas cleanup with selected commercial and full-size nickel-based catalysts. *Industrial & Engineering Chemistry Research* 2000; 39 (5): 1143-1154. <https://doi.org/10.1021/ie990738t>
- [41] Coll R, Salvadó J, Farriol X, Montané D. Steam reforming model compounds of biomass gasification tars: conversion at different operating conditions and tendency towards coke formation. *Fuel Processing Technology* 2001; 74 (1): 19-31. [https://doi.org/10.1016/S0378-3820\(01\)00214-4](https://doi.org/10.1016/S0378-3820(01)00214-4)
- [42] Garcia L, French R, Czernik S, Chornet E. Catalytic steam reforming of bio-oils for the production of hydrogen: effects of catalyst composition. *Applied Catalysis A: General* 2000; 201 (2): 225-239. [https://doi.org/10.1016/S0926-860X\(00\)00440-3](https://doi.org/10.1016/S0926-860X(00)00440-3)
- [43] Corella J, Orío A, Aznar P. Biomass gasification with air in fluidized bed: reforming of the gas composition with commercial steam reforming catalysts. *Industrial & Engineering Chemistry Research* 1998; 37 (12): 4617-4624. <https://doi.org/10.1021/ie980254h>
- [44] Huízar-Félix AM, Hernández T, de la Parra S, Ibarra J, Kharisov B. Sol-gel based Pechini method synthesis and characterization of Sm<sub>1-x</sub>CaxFeO<sub>3</sub> perovskite 0.1 ≤ x ≤ 0.5. *Powder Technology* 2012; 229: 290-293. <https://doi.org/10.1016/J.POWTEC.2012.06.057>
- [45] Cousin P, Ross RA. Preparation of mixed oxides: a review. *Materials Science and Engineering: A* 1990; 130 (1): 119-125. [https://doi.org/10.1016/0921-5093\(90\)90087-J](https://doi.org/10.1016/0921-5093(90)90087-J)
- [46] Navas D, Fuentes S, Castro-Alvarez A, Chavez-Angel E. Review on sol-gel synthesis of perovskite and oxide nanomaterials. *Gels* 2021; 7 (4): 275. <https://doi.org/10.3390/GELS7040275>
- [47] Hosseini SA, Salari D, Niaei A, Oskoui SA. Physical-chemical property and activity evaluation of LaB<sub>0.5</sub>Co<sub>0.5</sub>O<sub>3</sub> (B=Cr, Mn, Cu) and LaMnxCo<sub>1-x</sub>O<sub>3</sub> (x=0.1, 0.25, 0.5) nano perovskites in VOC combustion. *Journal of Industrial and Engineering Chemistry* 2013; 19 (6): 1903-1909. <https://doi.org/10.1016/j.jiec.2013.02.034>



- [48] Luo Y, Wang K, Chen Q, Xu Y, Xue H et al. Preparation and characterization of electrospun La(1-x)Ce(x)CoO(δ): application to catalytic oxidation of benzene. *Journal of Hazardous Materials* 2015; 296: 17-22. <https://doi.org/10.1016/j.jhazmat.2015.04.031>
- [49] Royer S, Bérubé F, Kaliaguine S. Effect of the synthesis conditions on the redox and catalytic properties in oxidation reactions of LaCo1-xFexO3. *Applied Catalysis A: General* 2005; 282 (1-2): 273-284. <https://doi.org/10.1016/J.APCATA.2004.12.018>
- [50] Levasseur B, Kaliaguine S. Effects of iron and cerium in La1-yCeyCo1-xFexO3 perovskites as catalysts for VOC oxidation. *Applied Catalysis B: Environmental* 2009; 88 (3-4): 305-314. <https://doi.org/10.1016/J.APCATB.2008.11.007>
- [51] Xu S, Wang X. Highly active and coking resistant Ni/CeO2-ZrO2 catalyst for partial oxidation of methane. *Fuel* 2005; 84 (5): 563-567. <https://doi.org/10.1016/J.FUEL.2004.10.008>
- [52] Kirumakki SR, Shpeizer BG, Sagar GV, Chary KVR, Clearfield A. Hydrogenation of naphthalene over NiO/SiO2-Al2O3 catalysts: structure-activity correlation. *Journal of Catalysis* 2006; 242 (2): 319-331. <https://doi.org/10.1016/j.jcat.2006.06.014>
- [53] Zhao A, Ying W, Zhang H, Ma H, Fang D. Ni-Al2O3 catalysts prepared by solution combustion method for syngas methanation. *Catalysis Communications* 2012; 17: 34-38. <https://doi.org/10.1016/j.catcom.2011.10.010>
- [54] López-Fonseca R, Jiménez-González C, de Rivas B, Gutiérrez-Ortiz JI. Partial oxidation of methane to syngas on bulk NiAl2O4 catalyst. Comparison with alumina supported nickel, platinum and rhodium catalysts. *Applied Catalysis A: General* 2012; 437-438: 53-62. <https://doi.org/10.1016/J.APCATA.2012.06.014>
- [55] Ho S-C, Chou T-C. The role of anion in the preparation of nickel catalyst detected by TPR and FTIR spectra. *Industrial & Engineering Chemistry Research* 1995; 34 (7): 2279-2284. <https://doi.org/10.1021/ie00046a009>
- [56] Alberton AL, Souza MMVM, Schmal M. Carbon formation and its influence on ethanol steam reforming over Ni/Al2O3 catalysts. *Catalysis Today* 2007; 123 (1-4): 257-264. <https://doi.org/10.1016/j.cattod.2007.01.062>
- [57] Hou Z, Yokota O, Tanaka T, Yashima T. Characterization of Ca-promoted Ni/α-Al2O3 catalyst for CH4 reforming with CO2. *Applied Catalysis A: General* 2003; 253 (2): 381-387. [https://doi.org/10.1016/S0926-860X\(03\)00543-X](https://doi.org/10.1016/S0926-860X(03)00543-X)
- [58] Calisan A, Uner D. Diversifying solar fuels: a comparative study on solar thermochemical hydrogen production versus solar thermochemical energy storage using Co3O4. In: Demirci Sankir N, Sankir M (editors). *Solar Fuels*. Hoboken, NJ, USA: Wiley, 2023, pp. 137-157.
- [59] Paryjczak T, Farbotko JM, Jóźwiak KW. Temperature-programmed reduction and oxidation of bimetallic Pd-Ni/Al2O3 catalysts. *Reaction Kinetics and Catalysis Letters* 1982; 20: 227-231. <https://doi.org/10.1007/BF02063614>
- [60] Zaera F. An organometallic guide to the chemistry of hydrocarbon moieties on transition metal surfaces. *Chemical Reviews* 1995; 95 (8): 2651-2693. <https://doi.org/10.1021/CR00040A003>
- [61] Batiot-Dupeyrat C, Valderrama G, Meneses A, Martinez F, Barrault J et al. Pulse study of CO2 reforming of methane over LaNiO3. *Applied Catalysis A: General* 2003; 248 (1-2): 143-151. [https://doi.org/10.1016/S0926-860X\(03\)00155-8](https://doi.org/10.1016/S0926-860X(03)00155-8)
- [62] Khoja AH, Anwar M, Shakir S, Mehran MT, Mazhar A et al. Thermal dry reforming of methane over La2O3 co-supported Ni/MgAl2O4 catalyst for hydrogen-rich syngas production. *Research on Chemical Intermediates* 2020; 46: 3817-3833. <https://doi.org/10.1007/s11164-020-04174-z>
- [63] Yang Eh, Moon DJ. CO2 reforming of methane over NiO/La2O3 catalyst without reduction step: effect of calcination atmosphere. *Topics in Catalysis* 2017; 60: 697-705. <https://doi.org/10.1007/s11244-017-0779-z>

## Supplementary information

S1. The reasoning behind the two-step calcination used for the preparation of  $\text{LaCoO}_3$  via sol-gel based Pechini method

In the preparation of  $\text{LaCoO}_3$  by citrate-based Pechini method, a two-step calcination was used to prevent a significant reduction of surface area and pore volume of the sample, which was observed when the sample was directly heated to  $650\text{ }^\circ\text{C}$  (Table S).

**Table S.** The comparison of surface area and pore volume obtained from two-stage heating and direct ramp up during calcination.

Method	BET surface area ( $\text{m}^2/\text{g}$ )	Pore volume ( $\text{cm}^3/\text{g}$ )
Two-stage calcination	5.91	0.005
Direct ramp up	0.15	0.001

The reason for the reduction in the surface area and pore volume was attributed to the pore collapse due to the fast decomposition of lanthanum and cobalt nitrates as evidenced by the weight loss observed at around  $350\text{ }^\circ\text{C}$  in TGA analysis (Figure S1). Due to this reason, we first heated the sample to the nitrate decomposition temperature  $350\text{ }^\circ\text{C}$  and waited at the related temperature for 3 h to slow down nitrate decomposition rate and to prevent the resulting pore collapse.

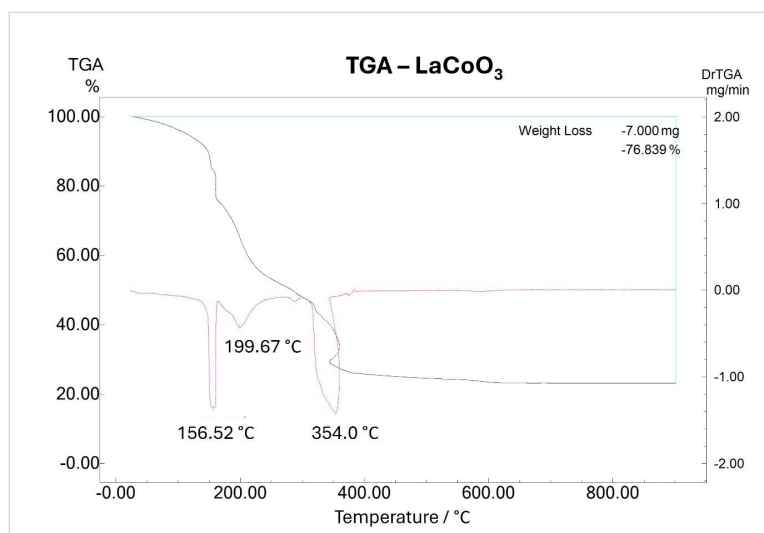


**Figure S1.** The TGA curve of the  $\text{LaCoO}_3$  prepared by citrate-based Pechini method before calcination.

S2. The reasoning behind the selection of calcination temperature for the  $\text{Ni}(15\text{ wt.}\%)/\gamma\text{-Al}_2\text{O}_3$  catalyst prepared by incipient wetness impregnation method

The  $\text{Ni}(15\text{ wt.}\%)/\gamma\text{-Al}_2\text{O}_3$  catalyst was prepared by incipient wetness impregnation method, which is commonly used technique for the preparation of catalysts due to technical simplicity, low costs and limited amount of waste. The method mainly consists of impregnation, drying, and calcination steps. The calcination step has a dramatic effect on the impurities sourced from precursors and crystal structure of catalysts. In the current study, TGA analysis was performed to determine a suitable calcination temperature for the  $\text{Ni}(15\text{ wt.}\%)/\gamma\text{-Al}_2\text{O}_3$  catalyst (Figure S2). TGA analysis shows that all nitrates are removed above  $500\text{ }^\circ\text{C}$ , as evidenced by no weight loss above this temperature interval.

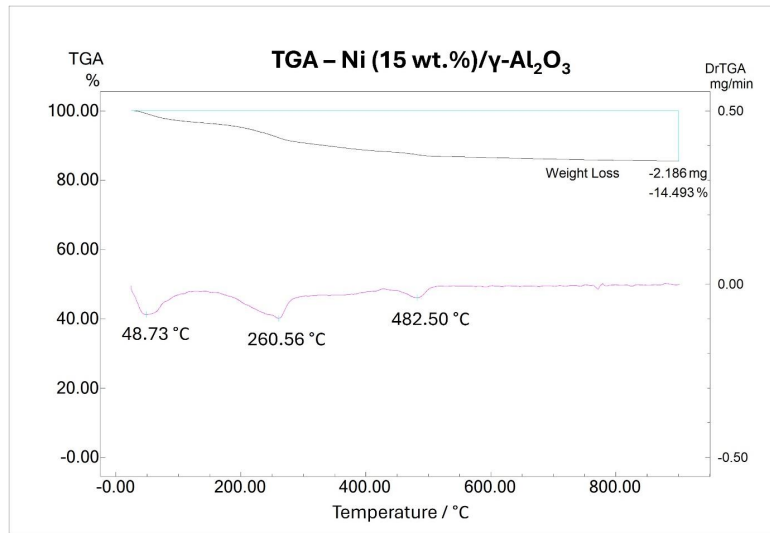


**Figure S2.** The TGA curve of the Ni(15 wt.)/ $\gamma$ -Al<sub>2</sub>O<sub>3</sub> catalyst prepared by incipient wetness impregnation method before calcination.

S3. The change of equilibrium constants of dry reforming reactions as a function of temperature

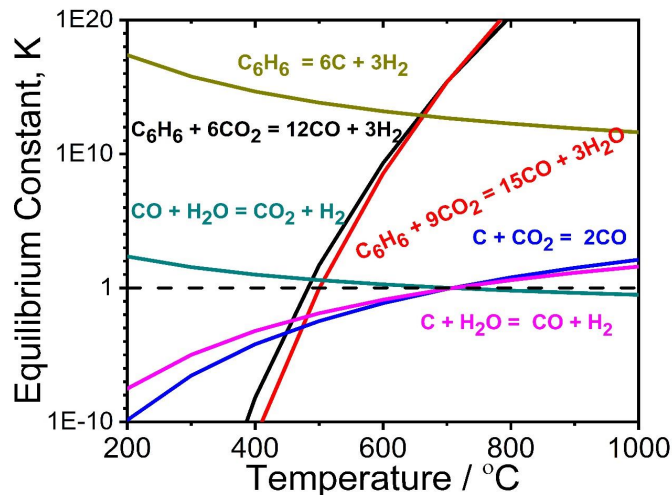


**Figure S3.** The change of equilibrium constants of reactions occurring at dry reforming conditions as a function of temperature.

S4. *N*<sub>2</sub> adsorption-desorption isotherms of LaCoO<sub>3</sub> and Ni/Al<sub>2</sub>O<sub>3</sub>

*N*<sub>2</sub> adsorption-desorption experiments show that the BET surface area and pore volume of the LaCoO<sub>3</sub> catalyst are almost 7-fold lower than those of the Ni(15 wt.)/ $\gamma$ -Al<sub>2</sub>O<sub>3</sub> catalyst while the average pore sizes of both catalysts are similar. The reason for the similarity in average pore diameters of catalysts while the difference in pore volume and surface area can be explained by the difference in tortuosity of the catalysts or the difference in their pore structure and shapes. The latter was analyzed by *N*<sub>2</sub> adsorption-desorption isotherms as seen in Figure S4. The Figure shows that the LaCoO<sub>3</sub> catalyst exhibits Type IV isotherm H4 hysteresis, which is an indication of narrow slit-like pore, while the Ni/Al<sub>2</sub>O<sub>3</sub> catalyst shows Type IV isotherm H2 hysteresis suggesting the presence of ink bottle shape pores. Since the average pore size in the current study was determined based on the BJH method assuming that all pores open-ended cylindrical, this may also lead to similar average pore size, but different pore volumes.

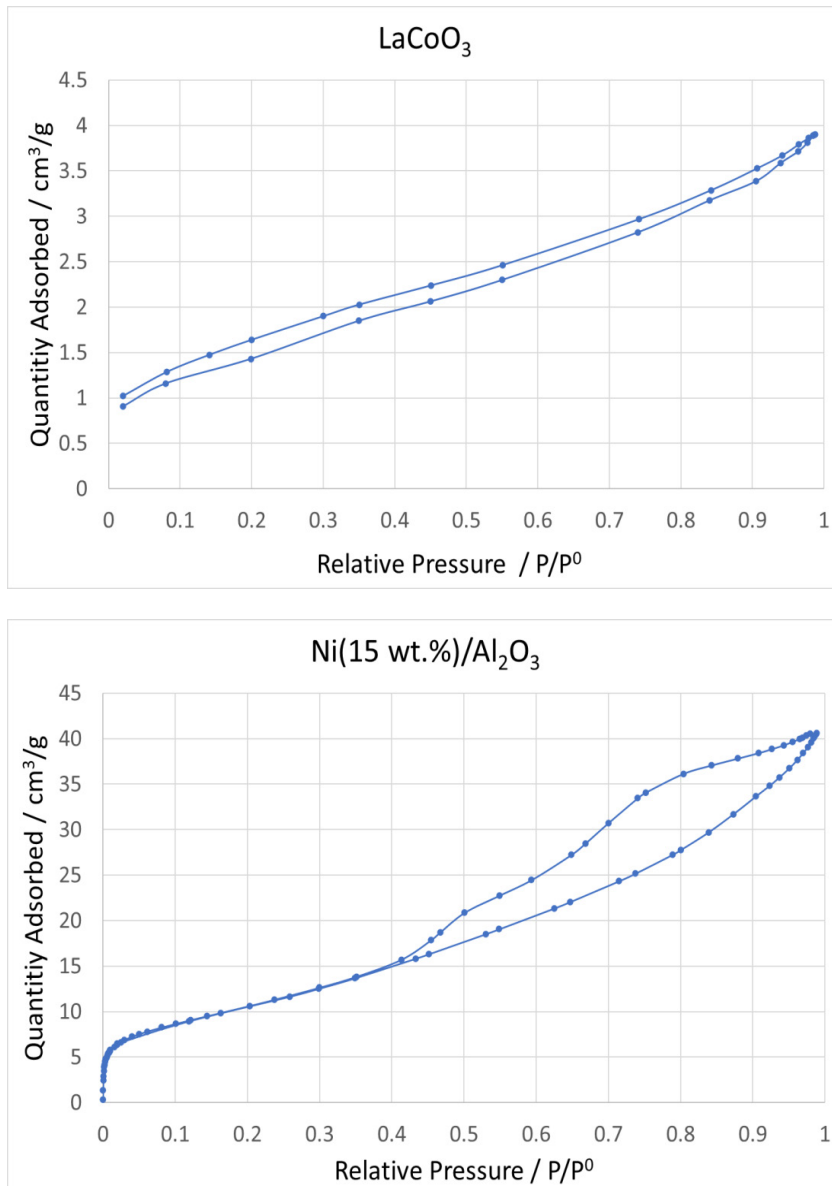
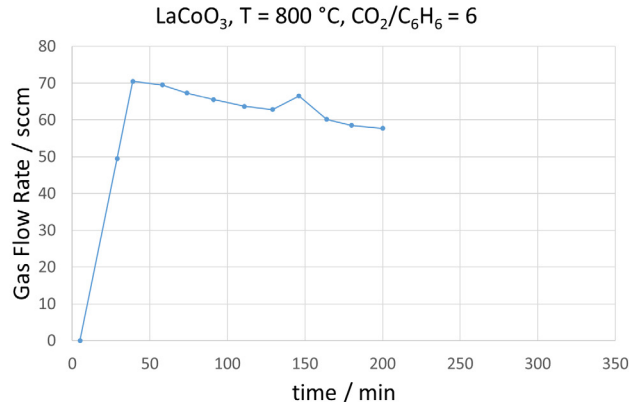


Figure S4. N<sub>2</sub> adsorption-desorption isotherms of LaCoO<sub>3</sub> (top) and Ni/Al<sub>2</sub>O<sub>3</sub> (bottom).

S5. The reasoning for the abnormality of conversion and yields in the first 50 min

CO<sub>2</sub> conversion and H<sub>2</sub> and CO yields change significantly with the first 50 min compared to those obtained after 50 min (Figures 4 and 5). The reason for this abrupt change in conversion and yields are related to the reaction setup used in this study. For all experiments, the position of powder catalyst was fixed tightly in the middle of reactor by quartz wool on both side of the catalyst bed to prevent any uncontrolled gas passage (e.g., free gas flow next to the reactor wall without contacting catalytic bed) through the reactor. This leads to pressure build-up in the first 50 min and limits gas flow at the reactor outlet, which is clearly seen in the gas flow rate measurement at the reactor outlet (Figure S5). When the pressure reaches a certain value, the gas blockage is removed, and the inlet and outlet gas flow rate are equalized. Since the outlet molar flow rate of each gas is calculated by the product of total gas flow rate and gas composition (determined by GC), the CO<sub>2</sub> conversion was found to be higher while H<sub>2</sub> and CO yields were determined to be lower than those observed after gas flow rate stabilization (i.e. after 50 min).



**Figure S5.** The variation of gas flow rate as function of time for the LaCoO<sub>3</sub> catalyst at the conditions of 800 °C and the CO<sub>2</sub>/C<sub>6</sub>H<sub>6</sub> ratio of 6.

S6. Equilibrium conversion and yields at different reactant ratios and temperatures

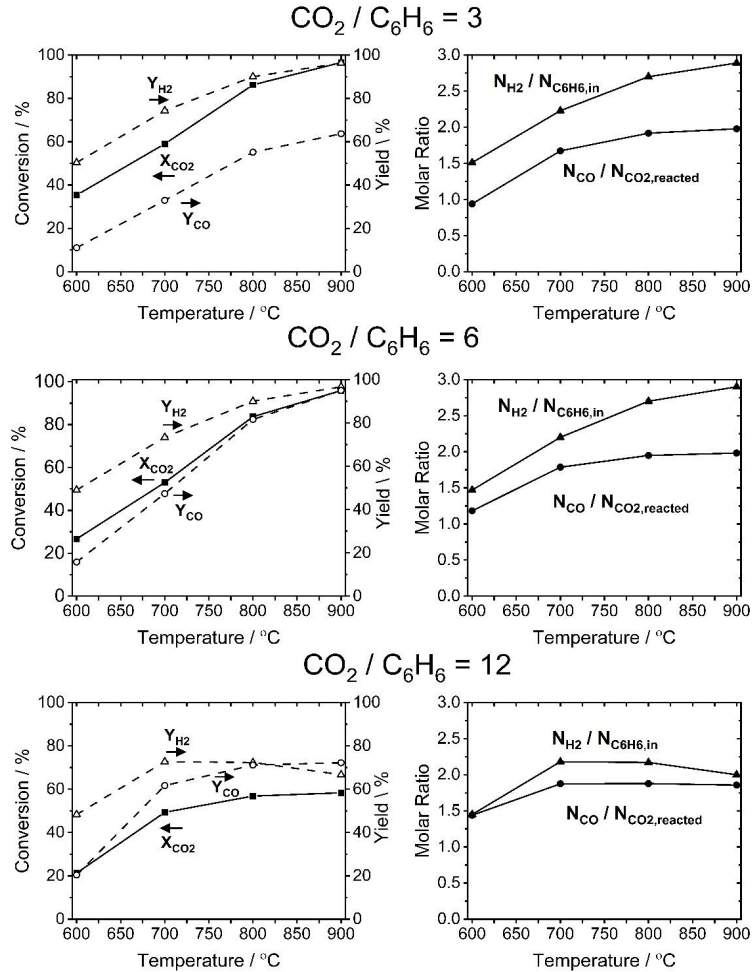


**Figure S6.** Equilibrium conversion of CO<sub>2</sub> and H<sub>2</sub> and CO yields (left panel) along with H<sub>2</sub>/N<sub>C<sub>6</sub>H<sub>6</sub>,in</sub> and CO/N<sub>CO<sub>2</sub>,reacted</sub> ratios at equilibrium conditions (right panel) determined based on Gibbs free energy minimization.

### S7. Postreaction characterization by TGA for confirmation of carbon formation

At the end of the dry reforming experiment, the used catalysts were collected from the reactor along with quartz wool and used for TGA analysis. Since it is difficult to separate the used catalyst from the quartz wool, the quartz wool was also included in the sample for TGA analysis. TGA analyses were performed between 25 and 900 °C with a heating rate of 10 °C/min under air atmosphere. TGA curves of the used  $\text{LaCoO}_3$  and  $\text{Ni}/\gamma\text{-Al}_2\text{O}_3$  catalyst obtained after the dry reforming experiment at 800 °C and at the  $\text{CO}_2/\text{C}_6\text{H}_6$  ratio of 6 are shown in Figures S7 and S8.

Figures show a typical weight loss between 500 and 700 °C for both catalysts, which is related to carbon oxidation. This clearly proves the carbon accumulation on the surface of catalysts during the dry reforming reaction. The total amounts of carbon accumulated on both catalyst surfaces were also calculated. The results show that carbon formation rate (determined by the total amount of carbon divided by the reaction duration) is higher on the  $\text{Ni}/\gamma\text{-Al}_2\text{O}_3$  catalyst compared to that on  $\text{LaCoO}_3$  catalyst, but this is not a reasonable comparison of the instant carbon yield of the catalysts since it is difficult to determine the exact reaction duration leading to carbon formation. When carbon builds up on the surface, it starts to block gas passage. The gas flow rate decreases slowly until the moment where an almost complete blockage occurs. Therefore, the averaging the carbon formation in time does not give correct assessment due to instabilities in the system.

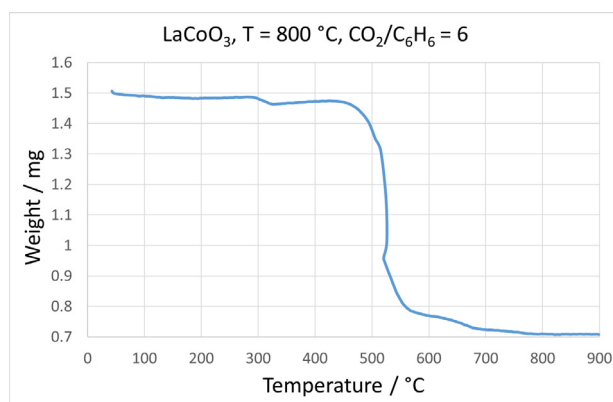


**Figure S7.** TGA analysis of the used  $\text{LaCoO}_3$  catalyst obtained after the dry reforming experiment at 800 °C and at the  $\text{CO}_2/\text{C}_6\text{H}_6$  ratio of 6.

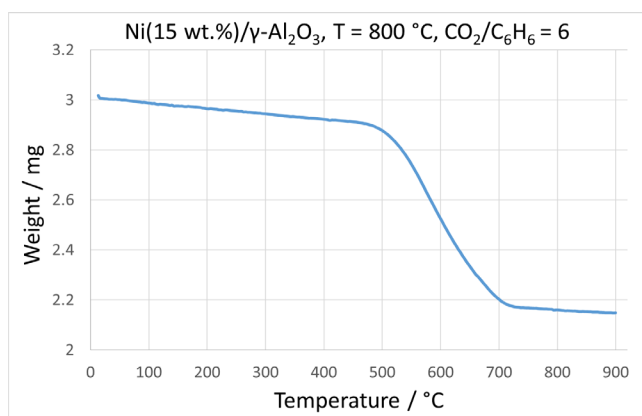


**Figure S8.** TGA analysis of the used  $\text{Ni}/\gamma\text{-Al}_2\text{O}_3$  catalyst obtained after the dry reforming experiment at 800 °C and at the  $\text{CO}_2/\text{C}_6\text{H}_6$  ratio of 6.

The TGA analysis was also performed for the used  $\text{LaCoO}_3$  and  $\text{Ni}/\gamma\text{-Al}_2\text{O}_3$  catalysts after the dry reforming experiment at 600 and 700 °C at the  $\text{CO}_2/\text{C}_6\text{H}_6$  ratio of 6. As seen from Figure S9, the TGA curve of the used  $\text{LaCoO}_3$  catalyst presents two weight increases at 300 and 395 °C. This is attributed to the oxidation of  $\text{La}_2\text{O}_3$  to  $\text{LaCoO}_{2.5}$  as seen in the TPO analysis (Figure 4). The related weight increase indicates that a part of the catalyst remains in the reduced form (i.e. Co and  $\text{La}_2\text{O}_3$ ) during dry reforming suggesting that a part of oxygen is exchanged to the surface for carbon oxidation. Different from the  $\text{LaCoO}_3$  catalyst, the related oxidation peaks are not present in the TGA curve of the  $\text{Ni}/\gamma\text{-Al}_2\text{O}_3$  catalyst. This explains the higher CO yields observed on the  $\text{LaCoO}_3$  catalyst compared to that of the  $\text{Ni}/\gamma\text{-Al}_2\text{O}_3$  catalyst. The TGA curves of both catalysts indicate weight decrease above 500 °C, which is related to oxidation of surface carbon. The relative weight decreases with respect to the initial weight before the carbon oxidation shows that the weight percentages of carbon in the used catalysts are 7.8% and 14.0% for  $\text{LaCoO}_3$  and  $\text{Ni}/\gamma\text{-Al}_2\text{O}_3$  catalysts, respectively. This suggests that the  $\text{LaCoO}_3$  catalyst is less prone to coke formation compared to the  $\text{Ni}/\gamma\text{-Al}_2\text{O}_3$  catalyst due to its high oxygen exchange capacity.

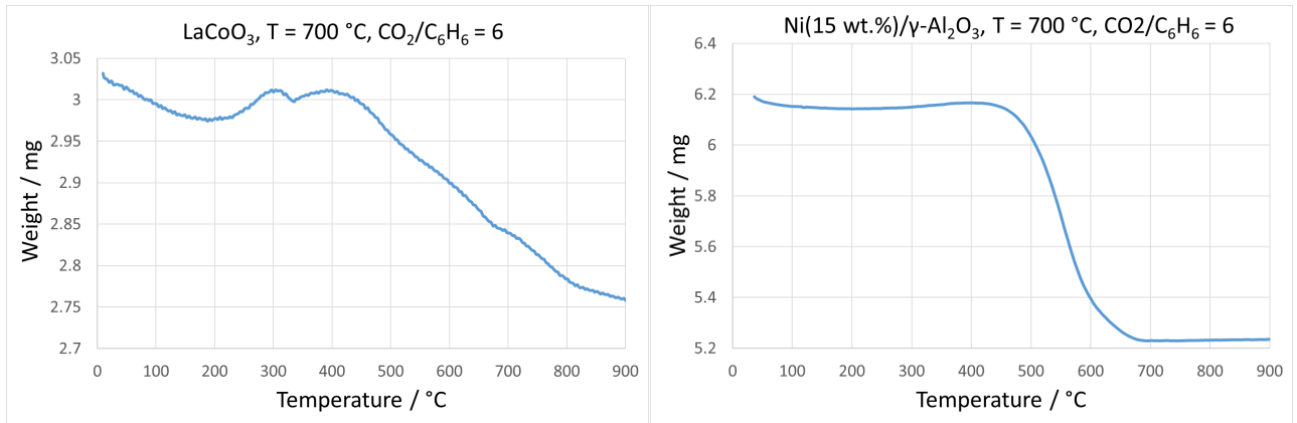


**Figure S9.** TGA analysis of the used  $\text{LaCoO}_3$  (left panel) and  $\text{Ni}/\gamma\text{-Al}_2\text{O}_3$  (right panel) catalysts obtained after the dry reforming experiment at 700 °C and at the  $\text{CO}_2/\text{C}_6\text{H}_6$  ratio of 6.